frontiers | Frontiers in Earth Science

TYPE Original Research
PUBLISHED 22 May 2024
DOI 10.3389/feart.2024.1387544

OPEN ACCESS

EDITED BY
Wenlong Ding,
China University of Geosciences, China

REVIEWED BY
Liang Qiu,
China University of Geosciences, China
Hu Li,
Southwest Petroleum University, China

*CORRESPONDENCE
Shi Chen,
chenshi4714@163.com

RECEIVED 18 February 2024
ACCEPTED 02 May 2024
PUBLISHED 22 May 2024

CITATION
Song X, Chen S, Zhang Y, Xie Z, Liang X, Yang M, Zheng M and Shi X (2024), Formation mechanism of the small-angle X-type strike-slip faults in deep basin and its controlling on hydrocarbon accumulation: a case study from the Tabei Uplift, Tarim Basin, NW China.
Front. Earth Sci. 12:1387544.
doi: 10.3389/feart.2024.1387544

Formation mechanism of the small-angle X-type strike-slip faults in deep basin and its controlling on hydrocarbon accumulation: a case study from the Tabei Uplift, Tarim Basin, NW China

Xingguo Song[1,2], Shi Chen[1,2]*, Yintao Zhang[3], Zhou Xie[3], Xinxin Liang[1,2], Minghui Yang[1,2], Mingjun Zheng[3] and Xukai Shi[3]

[1]National Key Laboratory of Petroleum Resources and Engineering, China University of Petroleum, Beijing, China, [2]College of Geosciences, China University of Petroleum, Beijing, China, [3]PetroChina Tarim Oilfield Company, Korla, China

In the central Tarim Basin, numerous hydrocarbon deposits were found along ultra-deep strike-slip faults, and its evolving progress and formation mechanism are research hotspots. The Paleozoic small-angle X-type strike-slip fault in the Tabei Uplift is the research subject in this article. Based on high-precision three-dimensional seismic data, three structural deformation layers were revealed: the rift system, weak strike-slip deformation and salt tectonics in the deep structural layer (Sinian–Middle Cambrian), the strong strike-slip deformation and karst-dissolution structure in the middle structural layer (Upper Cambrian–Middle Ordovician), and echelon normal faults in the shallow structural layer (Upper Ordovician–Carboniferous). The formation and evolution of strike-slip faults is jointly controlled by the distribution pattern of basement rift and the activities of surrounding orogenic belts, which can be divided into three stages. In the Middle to Late Cambrian, the initial subduction of the Paleo-Asian and Proto-Tethyan oceans precipitated the emergence of two sets of small-angle X-type strike-slip faults, striking NW and NE above the grooves of Precambrian rifts, influenced by local weak compressive stress. Affected by the closure of peripheral paleo-ocean, strike-slip faults deformed considerably in the Middle–Late Ordovician and were reactivated in the Silurian–Carboniferous, forming en-echelon normal faults in the shallow layer. The layered deformation structure of the strike-slip faults significantly affects the accumulation of hydrocarbons. The differential hydrocarbon enrichment of faults in the Tabei Uplift is collectively influenced by the distribution of source rocks and the migration of oil and gas. The topographical features of the Tabei Uplift, along with the distribution of strike-slip faults across tectonic units, have rendered the NE direction the preferential pathway for hydrocarbon migration. Additionally, impacted by the development of en echelon faults, the NE-trending faults offer superior conditions for

hydrocarbon preservation and charging condition, compared to the NW-trending faults.

KEYWORDS

X-type strike-slip fault, deformation layer, multistage evolution, formation mechanism, hydrocarbon accumulation, Tabei Uplift

1 Introduction

With the support of the latest 3D seismic data, a series of strike-slip faults were identified in seismic section profiles and various attribute map views, primarily buried in the Lower Paleozoic strata (˜4,500 m) and distributed around the Manjiaer Depression comprising a strike-slip fault system (˜4,000 km) (Li et al., 2013; Han et al., 2017; Deng et al., 2019; Wu et al., 2020a; Sun et al., 2021; Wang et al., 2021). The strike-slip faults in the Tarim Basin, which formed in the intraplate, are smaller in size (˜2 km) as the enormous strike-slip faults that formed at the plate boundaries, such as transform fault in the transform boundary and trench-linked and indent-linked strike-slip fault in the convergent boundary (Harding, 1974; Deng et al., 2019; Neng, et al., 2022). CNPC (China National Petroleum Corporation) and SINOPEC (Sinopec group) have made several commercial discoveries around strike-slip faults, including Halahatang, Tahe, Shunbei, Fuman, and Tazhong oil/gas fields, demonstrating that hydrocarbon accumulation was controlled by strike-slip faults (Jiao, 2018; Tian et al., 2021; Deng et al., 2022).

Many researchers have studied the spatial pattern, evolution process, and dynamics of the strike-slip faults in the central Tarim Basin. The characteristics of strike-slip faults vary in layers, with vertical strike-slip faults predominating in the deeper strata and en echelon normal faults characterizing the shallower layers (Han et al., 2017; Wu et al., 2020b; Deng et al., 2021). These faults display clear zoning features across different structural units (Deng et al., 2019; Chen et al., 2024), manifesting as unique fault systems within the Tabei Uplift, the Tazhong Uplift, and the Manxi Low Uplift. They are marked by segmented deformation, giving rise to a variety of patterns, including linear, braided, horsetail, and feather-like configurations (Neng et al., 2022; Shen et al., 2022; Yao et al., 2023). The evolution of strike-slip faults is indicative of multiple stages, but there is ongoing debate among scholars regarding the inception of their activity. The consensus suggests that strike-slip fault activity began in the Middle to Late Ordovician (Wang et al., 2020; Sun et al., 2021; Deng et al., 2022; Wu et al., 2019), but the latest research points to the possibility that their activity may date back to the Cambrian (Teng et al., 2020; Liu et al., 2023; Chen et al., 2024).

According to the Coulomb fracture criterion, the dihedral angle between X-type faults and fractures is 60°, with the bisector indicating the direction of the maximum principal stress (Anderson, 1951; Morley, 2014). However, in both natural settings and laboratory conditions, it has been observed that the dihedral angle deviates from 60° (Wu et al., 2018; Li et al., 2019; Fan et al., 2024), and those with a mean value significantly deviates below 60° are designated as low-angle or small-angle X-type faults and fractures in this paper. The Tabei Uplift is in the northern part of the Tarim Basin, distributing petroliferous strike-slip faults, characterized by small-angle X-type strike-slip faults (Wu et al., 2018; Deng et al., 2018). Regarding the formation mechanism of small-angle X-type faults, most authors considered that it belongs to pure shear deformation controlled by the N–S compression stress in the Middle Ordovician (Wu et al., 2018; Deng et al., 2018; Ma et al., 2019; Wu et al., 2021). However, the mechanism of the small dihedral angles of these X-type faults is still controversial. Some researchers have proposed confining pressure may influence the dihedral angles, which expand as the confining pressure intensifies (Ramsey and Chester, 2004; Ismat, 2015). Others suggested that lithology may be the controlling factor (Deng et al., 2018, 2019), the friction coefficient in varied lithology rocks differs (Mandl, 2000). While, some researchers found that the X-type faults developed asymmetrically in the Tabei Uplift, and the dihedral angle is related to the development of NW trending faults (Wu et al., 2018; Wu et al., 2020a). Furthermore, the preexisting basement structures are widespread in the center of Tarim basin (Yi et al., 2020; Chen et al., 2022), and the research in the Tazhong Uplift has demonstrated that pre-existing basement structures exert a significant control over the development of strike-slip faults (Han et al., 2017), but the impact of the basement structures on the development of strike-slip faults in the Tabei Uplift remains unclear. In addition, the Tabei Uplift is rich in oil and gas, but there is significant difference in the hydrocarbon enrichment in the NE- and NW- trending strike-slip fault, some author proposed that the reactivation of strike-slip faults might be the dominant factor (Deng et al., 2018, 2019; Chen et al., 2023). However, the impact of the layered deformation structure, multistage evolution, and the distribution of source rock on the differential hydrocarbon enrichment in the Tabei Uplift remains uncertain, and further research is still needed.

Based on the latest seismic data from CNPC survey of the Tabei Uplift and its surroundings, we have interpreted the geometry of the strike-slip faults and identified their active stages. By reconstructing the Paleozoic basement's paleotectonic feature, the paleo-stress field has been restored, and the formation mechanisms and evolution model of the X-type strike-slip faults were established, considering its Precambrian basement structure and the activities of orogenic belt. Integrating deformation patterns, the evolutionary timeline, and source rock distribution, the key factors influencing the differential hydrocarbon distribution within the Tabei Uplift were proposed. Research indicates that the development and evolution of the small-angle X-shaped strike-slip faults are jointly controlled by the basement structure and the evolution of the surrounding orogenic belts. Furthermore, the differential enrichment characteristics of oil and gas in the strike-slip faults of the Tarim Basin are collectively influenced by the source rock deposition center, the topographical features of the Tabei Uplift, and the layered deformation structure of the faults.

This study aims to 1) address the deformation patterns and active stages of the strike-slip fault, 2) discuss the formation mechanism and evolution history of small-angle X-type strike-slip fault system, and 3) propose the role of strike-fault on the accumulation of

hydrocarbons and the controlling factors of differential enrichment of oil and gas.

2 Geological setting

The Tarim Basin is China's largest petroliferous basin, approximately 56,000 km^2 (Jia, 1997). It lies northwest of China, surrounded by the Tianshan, Kunlun, and Altyn Orogenic Belts. The basin underwent a complicated evolution history and is characterized as a typical superimposed basin (Tang, 1994; Jia and Wei, 2002; He et al., 2005,2006). It comprises seven major structural units: the Kuqa Depression, the Tabei Uplift, the North Depression belt (the Manxi Low Uplift, the Manjiaer and Awati Depression), the Central Uplift belt, the Southwest Depression, the Southeast Uplift, and the Southeast Depression (Figure 1A). The Tabei Uplift spans more than 500 km in an east–west orientation and is in the northern part of the basin. It borders the Kuqa Depression to the north and transitions into to the Manxi Low Uplift towards the south (Figure 1B).

Affected by the evolution of the surrounding orogenic belt, the Paleozoic strata in the Tarim Basin exhibit multiple lithologies (Figure 2). Marine carbonate rock developed in the Cambrian–Middle Ordovician, including dolomite (Cambrian to Lower Ordovician) and limestone (Middle Ordovician), with gypsum and salt layers widely distributed in the Middle Cambrian. Mudstones are developed in the Upper Ordovician, and the clastic rocks with intercalated limestone are widespread in the Tabei Uplift from the Silurian to the Carboniferous, their thickness increase from the Manxi Low Uplift to Tabei Uplift (Figure 3). In the Permian, volcanic activity was extensive in the basin, and volcanic rocks were widely distributed (Yang et al., 2013; Li et al., 2014; Xu et al., 2021).

From the Precambrian to Permian, the Tarim Basin shows multistage, strong tectonic action (Nakajima et al., 1990; Jia, 1997; Jia and Wei, 2002; Li et al., 2013; Gao and Fan, 2014) that resulted in rift, thrust, and strike-slip fault systems (Figure 3), with the evolution of orogenic belts surrounded. The crystalline basement was formed in the Archean–Early Neoproterozoic (Zhu et al., 2017; Wu G. H. et al., 2018; Wu et al., 2020c). Early in the Archaeozoic and Proterozoic, the Tarim Block separated from the Rodinia supercontinent, with rift distributed in the Precambrian (Figure 3), and the paleo oceans formed around the block (Jia, 1997; Mattern and Schneider, 2000; Wang, 2004). The Tarim Basin was in a passive continental margin and subject to an extensional regional tectonic stress field during the Cambrian and Early Ordovician (Li et al., 2013; He et al., 2016; Jia et al., 2021; Neng et al., 2022). From Middle Ordovician to Late Ordovician, due to the subduction of the ancient Kunlun Ocean (Zhang et al., 2002; Li et al., 2009), the Tarim Basin transformed to an active margin, and the Tabei Uplift formed (Li et al., 1996; Wang, 2004). From the Silurian to the Devonian, folds and thrusts were developed intensely in the Arkin tectonic domain (Yang et al., 2005; Liu et al., 2007). Furthermore, the South Tianshan Ocean subducted and closed in a scissor-like form in the Carboniferous, and severe deformation occurred in the Tianshan orogenic belt (Figure 1A) (Gao et al., 2006). A significant igneous province occurred in the basin due to widespread volcanism caused by the intense activity of the Permian mantle plume (Yang et al., 1996; Chen et al., 2006; Li et al., 2013).

Influenced by the Precambrian basement structure, the distribution feature of the carbonate platform margin and evolution history of orogenic belts (Yang et al., 2020; Chen et al., 2024), the Tabei Uplift developed an extensive strike-slip fault system that could be separated into three sections by regional strike-slip faults like F_I5 (Figure 1B). In the western part, faults in a NW–SE orientation dominate. Most cut through the Manxi Low Uplift or extend to the Tazhong Uplift in the south and connect to F_I5. In the middle part, in the Halahatang Sag, two sets of strike-slip faults exhibit a NW and NE trend, intersecting and ending in the Manxi Low Uplift southward as an X-shape with dihedral angles from 20° to 40°. Most strike-slip faults in the eastern part are oriented toward NE, and several regional strike-slip faults exceed 200 km southward into the Manxi Low Uplift.

3 Data and methods

In this study, the Tarim oilfield company provided a high-solution 3D seismic survey covering the Halahatang area of $^>$1,500 km^2 for the fine structure interpretation of strike-slip fault systems (Figure 4), and all seismic data are processed on the Landmark software. Reflection interfaces were easily identified in the seismic section calibrated by several deep wells and well logs in the area. The poststack time-migration 3D seismic data used here are favorable for structural interpretation. The 3D coherence, curvature, and other seismic attributes are used to recognize faults in map view, with slices of primary reflection interfaces from the Cambrian to the Permian, such as the bottom of the Upper Cambrian ($T\mathfrak{E}_3$) and the bottom of the Upper Ordovician (TO_3), indicating the plane features of faults in various depths. In section view, deformations of the interfaces, such as cut-off (vertical displacement of $^>$5 m) and bending, are the signatures for fault identification; furthermore, chaotic seismic reflection configurations and fault-karst reflections indicate fault damage zones. The interfaces, relatively stable and seldom affected by later denudation, such as $T\mathfrak{E}_1$ (Figures 2, 3), can restore the map of paleotectonic of the interface during tectonic evolution, accompanied by residual strata thickness in each period. Besides, the characteristics of the paleostress field of the region can be restored by analyzing the migration and evolution in time and space based on the map of paleotectonic.

Seismic interpretation, combined with the spatial distribution of unconformities, the growth of strata, and the evolution history of adjacent orogenic belts, can help clarify the stages of evolution of strike-slip faults. Furthermore, a new viewpoint on the X-type strike-slip fault formation mechanism can be explored with characteristics of the basement structure.

4 Fault characteristics

4.1 Identifications of strike-slip faults

In section, map, and 3D views, the strike-slip faults have distinctive characteristics that set them apart from dip-slip faults. The primary fault planes of strike-slip faults typically developed vertically in seismic profiles and combined with the minor nearby

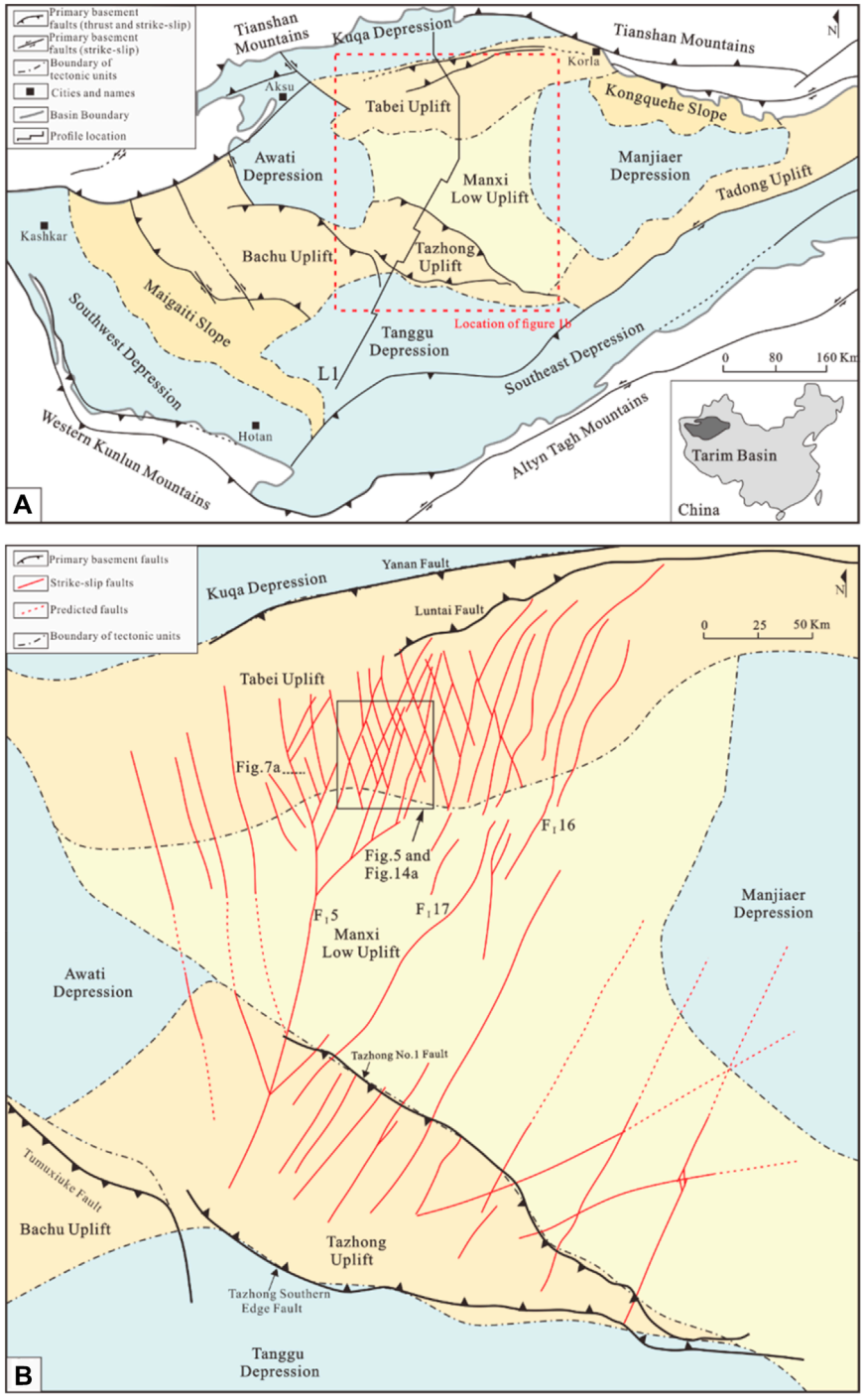

FIGURE 1
(A) Simplified distribution map of the tectonic units in the Tarim Basin [modified from Li et al. (2013), Deng et al. (2019)]; **(B)** enlarged view of the northern part of **(A)** showing the distribution of strike-slip faults at the bottom of the Upper Ordovician (the TO_3 interface) around the Tabei Uplift [modified from Wang Z. Y. et al. (2020)]; the background colors indicate tectonic units of different types: uplifts, low uplift, depressions, and slopes are shown in brown, yellow, blue, and orange, respectively.

faults to generate the flower structures, either positive or negative (Harding, 1974; Chritie-Blick and Biddle, 1985; Harding, 1985; Swanson, 2005). In map view, as the displacement occurred along the strike, the abrupt cut-off of markers, such as the relics of paleo rivers and facies of igneous rocks, presents across the fault planes (Ramadan et al., 2014). Strike-slip faults also frequently appear in various shapes, including linear, oblique, feather, en-echelon, X-shape, and broom-shape. Dolphin and ribbon effects in the 3D image help identify strike-slip faults (Graham et al., 1984; Harding, 1985; Romeo et al., 2005).

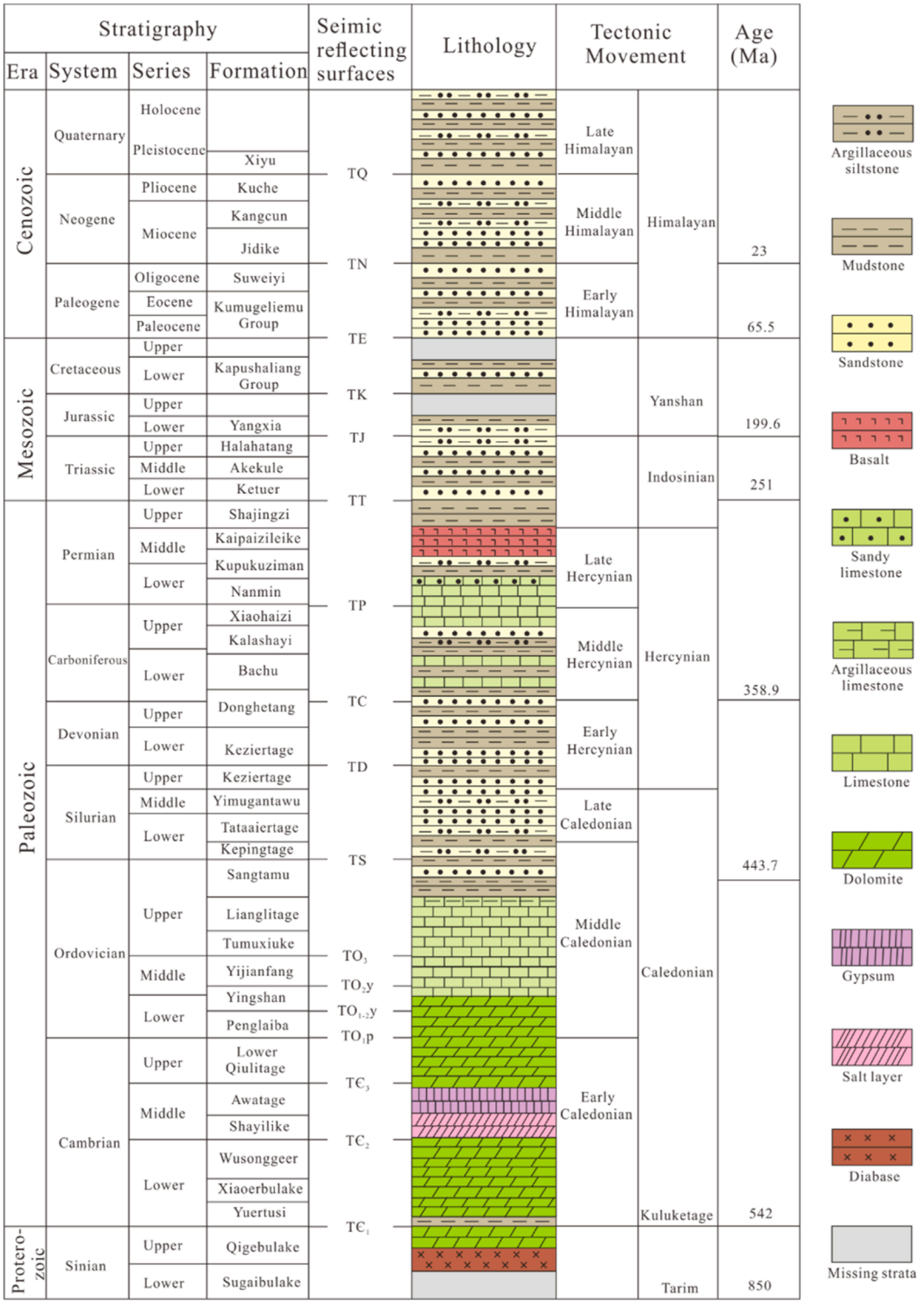

FIGURE 2
Chart showing the Tarim Basin stratigraphy, the seismic reflecting surfaces (horizons), and the timing of regional tectonic movements [modified from Deng et al. (2019), Neng et al. (2022)].

Interpretations of the Tabei Uplift (TO_3) reveal that most faults display a linear structure, while horsetail and en-echelon occurred sparsely across the Tabei Uplift at the tip of some strike-slip faults (Figure 5C). The seismic sections (Figure 6) across the Tabei Uplift show that most faults are subvertical and develop a flower structure with intense deformation near the bottom of Upper Ordovician, the seismic reflection interface of TO_3. In summary, the Tabei Uplift developed a

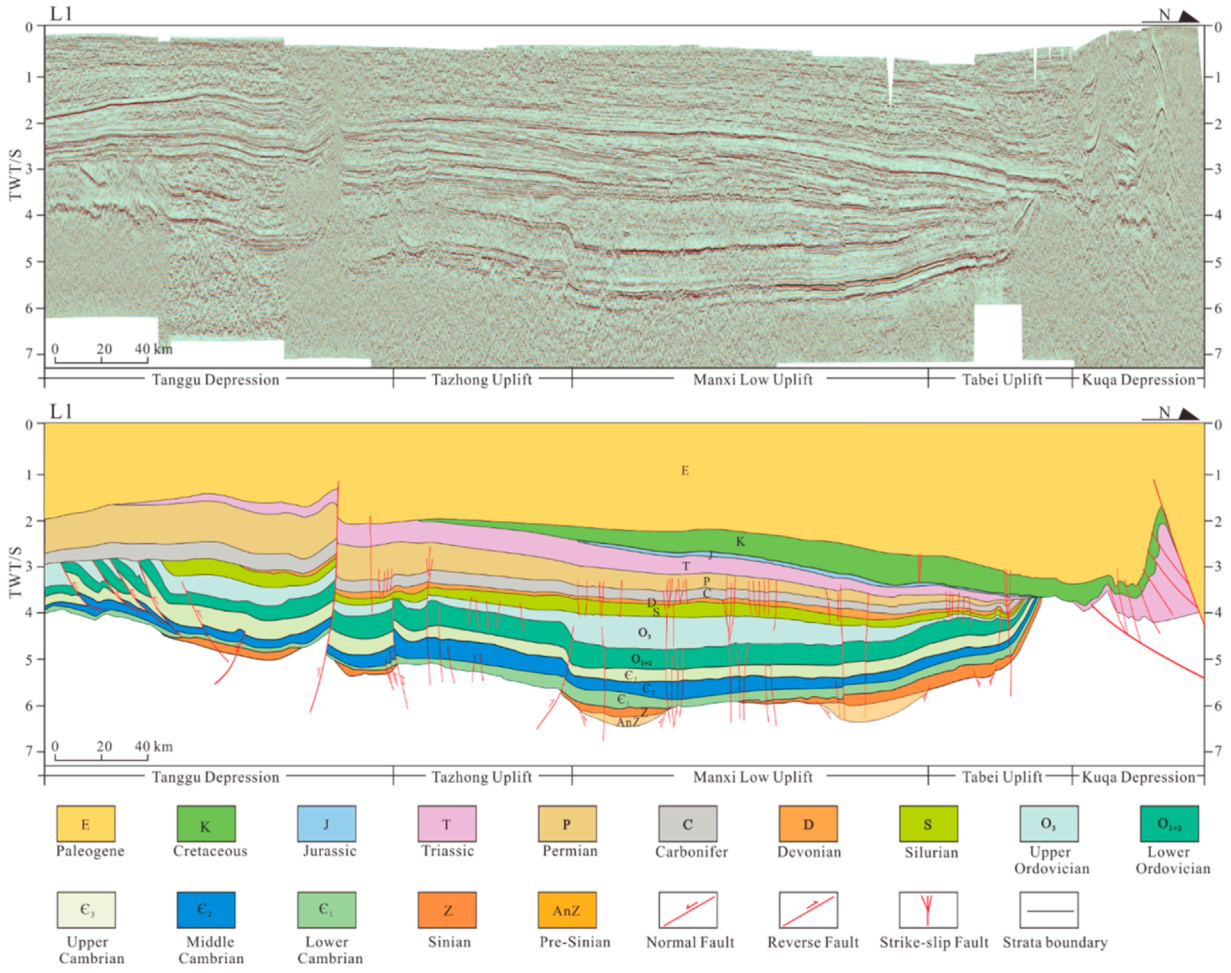

FIGURE 3
Regional profile of the Tarim Basin (L1 line in Figure 1A).

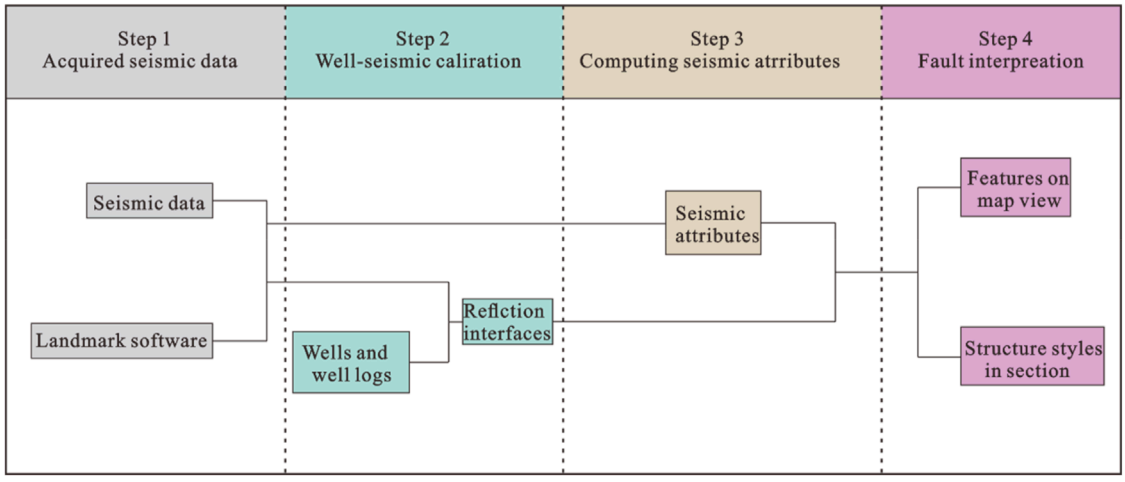

FIGURE 4
The flowchart of seismic interpretation.

complicated strike-slip fault system with severe deformation during the Paleozoic.

4.2 Distribution characteristics on map view

The complicated strike-slip fault system is distributed widely in the Tabei Uplift as two sets of intersected X-type faults (Figures 1, 5). The distribution patterns of the strike-slip system were identified in various interfaces, from deep to shallow, and present distinctive characteristics: the bottom of the Lower Cambrian ($T\mathcal{E}_1$), the bottom of the Upper Cambrian ($T\mathcal{E}_3$), the bottom of the Upper Ordovician (TO_3), and the bottom of the Silurian (TS).

The strike-slip faults appear segmented, linear, but intermittent on the coherence slices of interface $T\mathcal{E}_1$ (Figures 5A, E), where the NW-trending faults dominate the fault system with stronger activity and wider distribution. Strike-slip faults on the surface of $T\mathcal{E}_3$ share characteristics with the interface of $T\mathcal{E}_1$ but comprise longer linear fault segments. Meanwhile, NE-trending faults exhibit broader distributions and extend over longer planes compared to the $T\mathcal{E}_1$ interface (Figures 5B, F). Additionally, the initial configuration of the two sets of X-type faults, intersecting at a small angle (~40°), is discernible on the interface. The strike-slip faults are linear and longer but more continuous on the interface of TO_3, with intense activity (Figures 5C, G). Subordinate faults developed along the principal displacement zone of major faults, such as the Riedel shear, and displayed in horsetail splay, oblique, and feathered. The intersection relationship of these X-type faults indicates that the NE faults are left lateral, whereas the NW faults are right lateral. On the surface of TS (Figures 5D, H), en-echelon faults are displayed along the trending of deep strike-slip faults. Most en-echelon faults exhibit left-stepping in a NW linear configuration, and the average intersection angle with the underlying strike-slip faults is 45°, demonstrating that the en-echelon faults belong to T fractures (Tondi et al., 2012; Han et al., 2017; Deng et al., 2019), which develop when NW strike-slip faults are reactivated with dextral movements.

4.3 Structure styles in section

Several seismic profiles were selected to represent the features of fault systems in the Tabei Uplift (Figures 1B, 5, 6). The overall fault characteristics in the seismic sections, from north to south, are similar (Figures 6A–C), displaying layered deformation structure, from deep to shallow (Table 1). Three deformation layers were recognized: the deep structural layer (Sinian–Middle Cambrian, basement–$T\mathcal{E}_3$), the middle layer (Upper Cambrian–Middle Ordovician, $T\mathcal{E}_3$–TO_3), and the shallow layer (Upper Ordovician–Carboniferous, TO_3–TP).

The deep structural layer comprises the Sinian rift system, weak deformed strike-slip faults, and salt-related structures. On the seismic section, several normal faults in high-dip angles emerged in the Sinian rift system. The strike-slip faults display subvertical fault planes propagating from the basement, and many developed along the margin of normal faults or followed the preexisting fault planes (Figure 6B), showing that basement structures influenced the

TABLE 1 Structure styles of major faults in section.

Strike	Fault numbers	Structure styles in section		
		Deep structural layer	Middle structural layer	Shallow structural layer
NE	F4	Semi-flower structure Salt sag Linear shape strike-slip fault	Positive flower structure Semi-flower structure	—
	F8	Rift structure Linear shape strike-slip fault	Positive flower structure	—
	F10	Linear shape strike-slip fault	Positive flower structure Negative flower structure	—
	F15	Linear shape strike-slip fault	Linear shape strike-slip fault Semi-flower structure	—
NW	F6	Rift structure Linear shape strike-slip fault	Positive flower structure Semi-flower structure	Graben Half-graben
	F7	Salt dome Positive flower structure	Positive flower structure	Graben Complicate flower structure
	F9	Rift structure Salt dome Linear shape strike-slip fault	Positive flower structure Semi-flower structure Linear shape strike-slip fault	Graben Complicate flower structure
	F13	Rift structure Semi-flower structure Salt dome	Positive flower structure Negative flower structure	Graben

10.3389/feart.2024.1387544

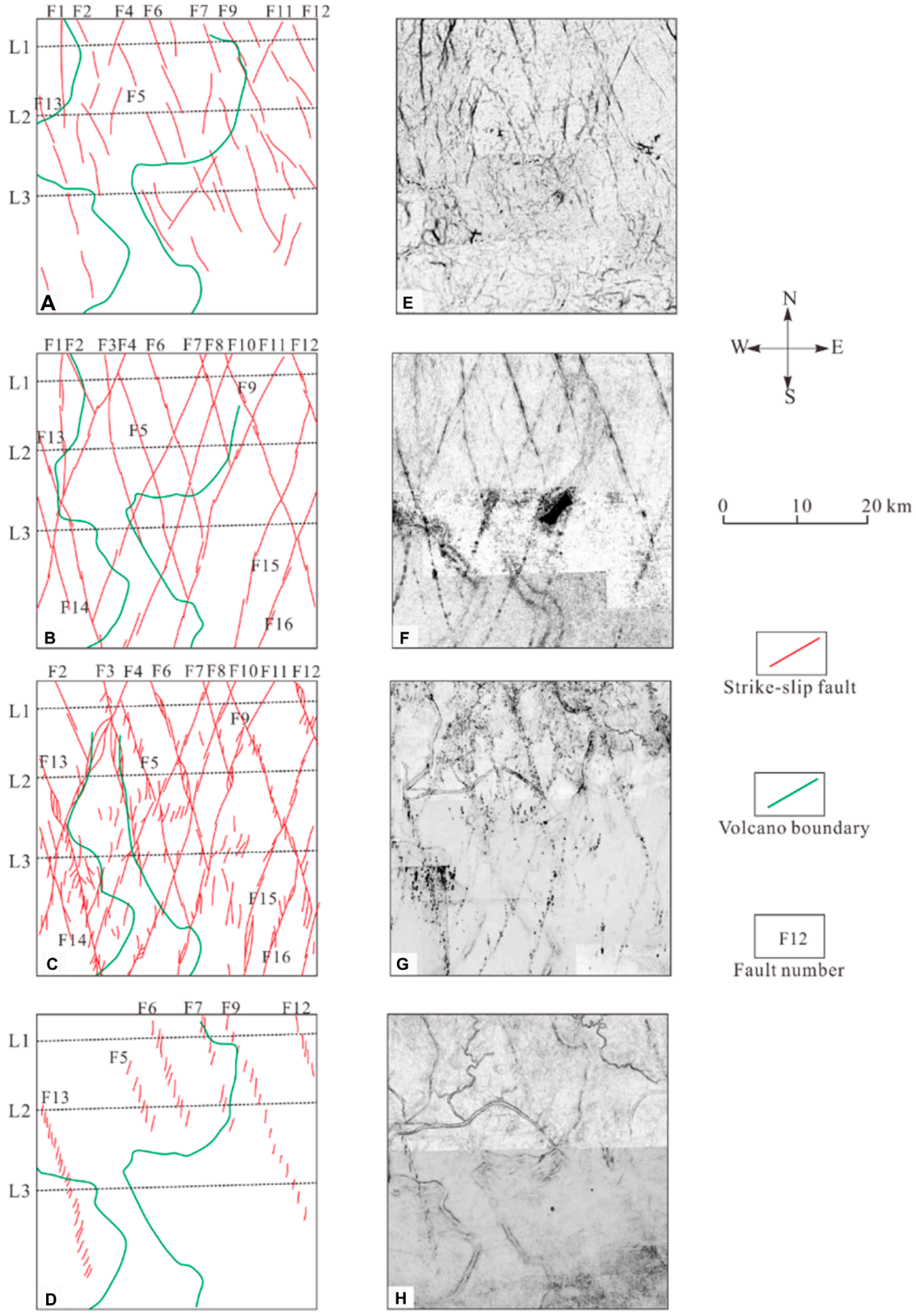

FIGURE 5
Interpreted fault systems **(A–F)** and corresponding uninterpreted coherence slices **(E–H)** of different seismic reflection surfaces of the Tabei Uplift (for location, see Figure 1B): **(A)** $T\epsilon_1$ reflection surface (bottom of the Lower Cambrian), **(B)** $T\epsilon_3$ reflection surface (bottom of the Upper Cambrian), **(C)** TO_3 reflection surface (bottom of the Upper Ordovician), **(D)** TS reflection surface (bottom of the Silurian).

10.3389/feart.2024.1387544

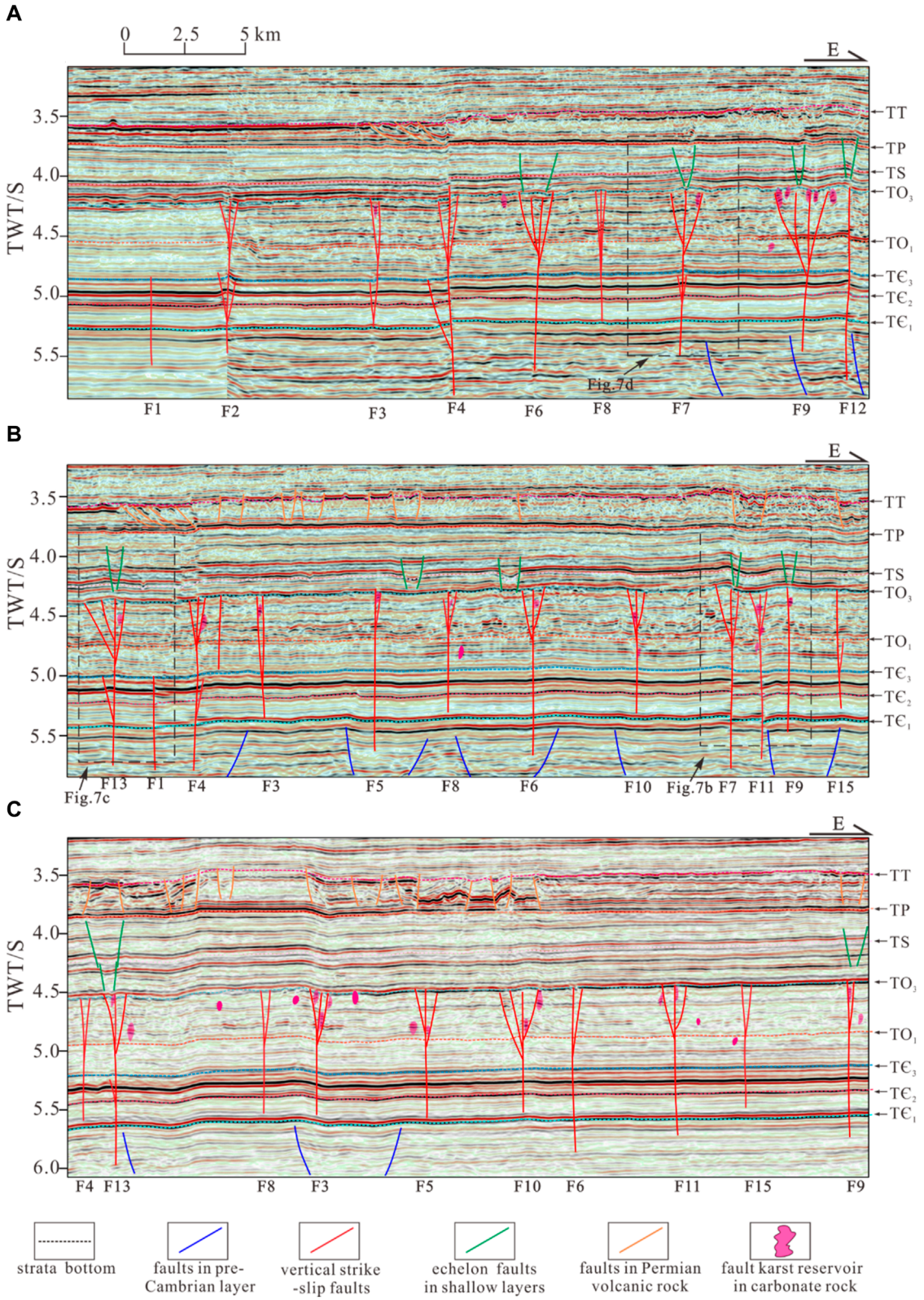

FIGURE 6
Characteristics of the layered deformation of typical 3D seismic profiles of the Tabei Uplift (for location, see Figure 4): **(A)** 3D seismic line of the northern part (L1), **(B)** 3D seismic line of the northern part (L2), and **(C)** 3D seismic line of the northern part (L3).

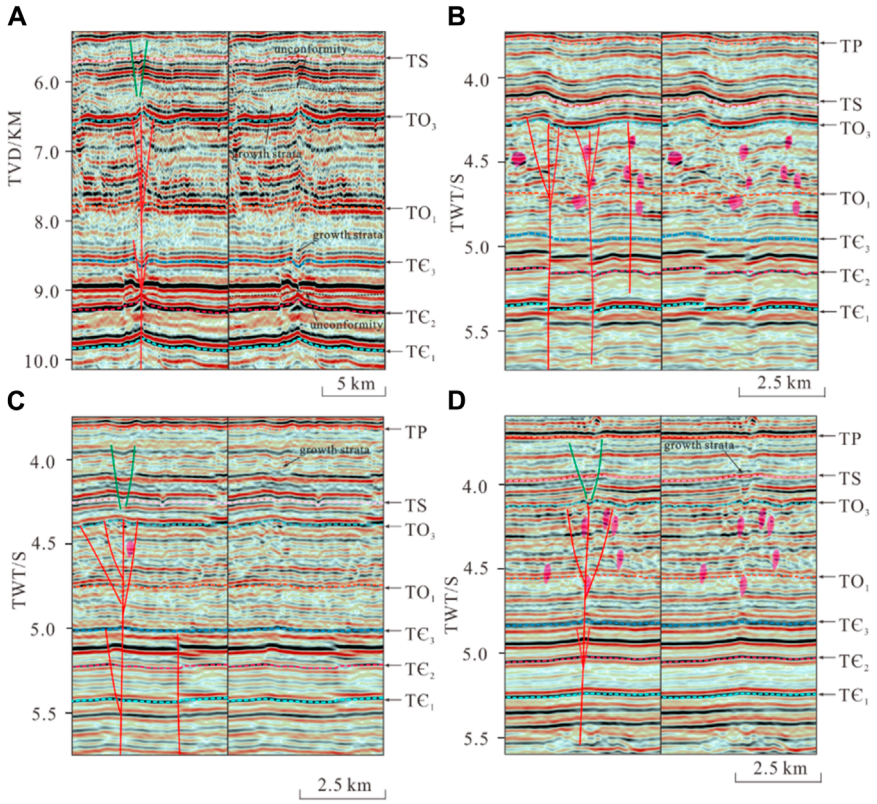

FIGURE 7
Typical 3D seismic profiles of multistage evolution (for location, see Figures 1B, 6): **(A)** Negative flower structure in the deep structural layer contrasted with the positive flower structure in the middle structural layer, **(B)** Fault displacement varied with depth and decrease from the Cambrian to Ordovician, **(C)** Strike-slip faults ended in the Middle Cambrian, **(D)** Fault-karst reflections were identified in the Upper Cambrian.

development of strike-slip faults. Besides, the faults inserted into the basement are more in the NW-trending than in the NE-trending. Some minor or secondary faults formed in the Lower–Middle Cambrian, connected to the major fault planar, and are interpreted as flower structures, such as F2 and F13 (Figures 6A, B). In response to localized tectonic stress alterations within the fault deformation zone and the distinctive physical characteristics of salt, the Middle Cambrian strata underwent a variety of deformational expressions, characterized by localized amplification and reduction in thickness, as exemplified by the emergence of salt domes and sag structures (Figure 6A, F4 and F7).

The middle structural layer, Upper Cambrian–Middle Ordovician, comprises strike-slip faults deformed intensely near the bottom of the Upper Ordovician (TO_3) and is expressed as a flower structure or linear shape. The fault planes predominantly terminate near the bottom of the Upper Ordovician (TO_3), with branching secondary faults extending downwards to the intersect with the primary fault. Anticlines and synclines developed in the carbonate strata, forming positive and negative flower structures (Figure 6A, F6, and F7). Some strike-slip faults were linear when they experienced weak deformation (Figure 6B and F15).

The shallow structural layer, Upper Ordovician–Carboniferous, comprises clastic rocks and develops normal faults, forming graben and half-graben. In some cases, the shallow normal fault penetrated through the Upper Ordovician strata, extending into the Ordovician carbonate rocks, and disrupted the underlying anticlines and positive flower structures below, resulting in the formation of complicated flower structure (Figure 6A, F9 and F7).

5 Active stage and deformation phase

Based on the detailed seismic interpretations of strike-slip faults, features of unconformities, growth strata in the deformation zone and distribution patterns of fault-karst reflections, three active Paleozoic stages of strike-slip faults were identified in the Paleozoic: Middle–Late Cambrian, Middle–Late Ordovician, and Silurian–Carboniferous.

The strike-slip faults were active in the Middle–Late Cambrian, as shown by various aspects below. The negative flower structure in the deep structural layer contrasted with the positive flower structure in the middle structural layer, exhibiting opposite superimposed feature (Figure 7A), suggests that they were formed under different tectonic stress and distinct periods, with evidence indicating significant fault activity during the Middle-Late Cambrian. Meanwhile, angular unconformities within the Middle Cambrian, along with growth strata that developed in the Upper Cambrian (Figure 7A), are associated with the formation of negative flower structures around the interface of $T\epsilon_3$ and the strata inside the deformation zone are thicker than those outside. Both of these features are related to intense fault activities in the Middle-Late

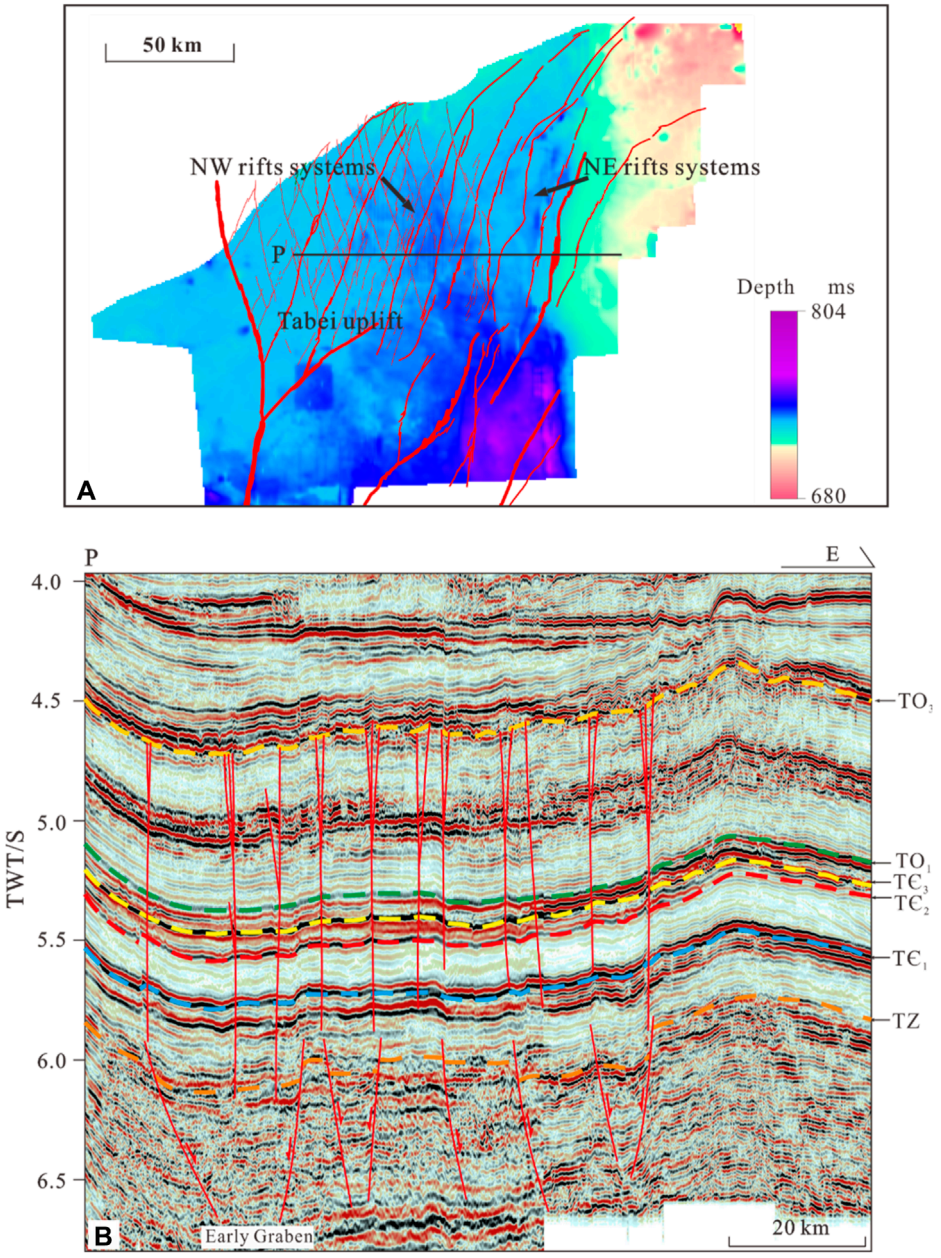

FIGURE 8
(A) The map of paleotectonic restoration of the Tabei Uplift of $T\epsilon_1$ in the late Early Cambrian and **(B)** the seismic profiles presenting the basement rift systems.

Cambrian. Fault-karst reflections were identified in the Upper Cambrian (Figures 7B, D), indicating the fault-related movement in the Late Cambrian (Neng et al., 2022). Some strike-slip faults ended in the Upper Cambrian or the Middle Cambrian (Figure 7C), failing to go upward to the bottom of the Upper Ordovician, showing that fault activity ended in the Middle and Late Cambrian. Strike-slip fault displacement varied with depth and decrease from the Cambrian to the Ordovician (Figure 7B), indicating that tectonic activity gradually diminished with the evolving processes.

The second active stage was in the Middle-Late Ordovician when the bottom of the Upper Ordovician (TO_3) underwent significant deformation. The vertical strike-slip faults terminated near the interface of TO_3, predominantly displaying positive flower structures within transpression tectonic stress fields (Figures 7A, D). Notably, the interface of TO_3 shows the most pronounced deformation amplitude (Figures 7A, C), and fault-karst reflection widespread beneath the TO_3 interface, suggesting that the strike-slip faults were intensely active at the end of Middle Ordovician. Furthermore, the strata between the interface of TO_3 and TS were deformed, with Growth strata unconformity occurred (Figure 7A), demonstrating that strike-slip fault activity persisted into the Late Ordovician.

The en-echelon normal faults, which formed in the shallow structural layer from the Silurian to the Carboniferous, are the

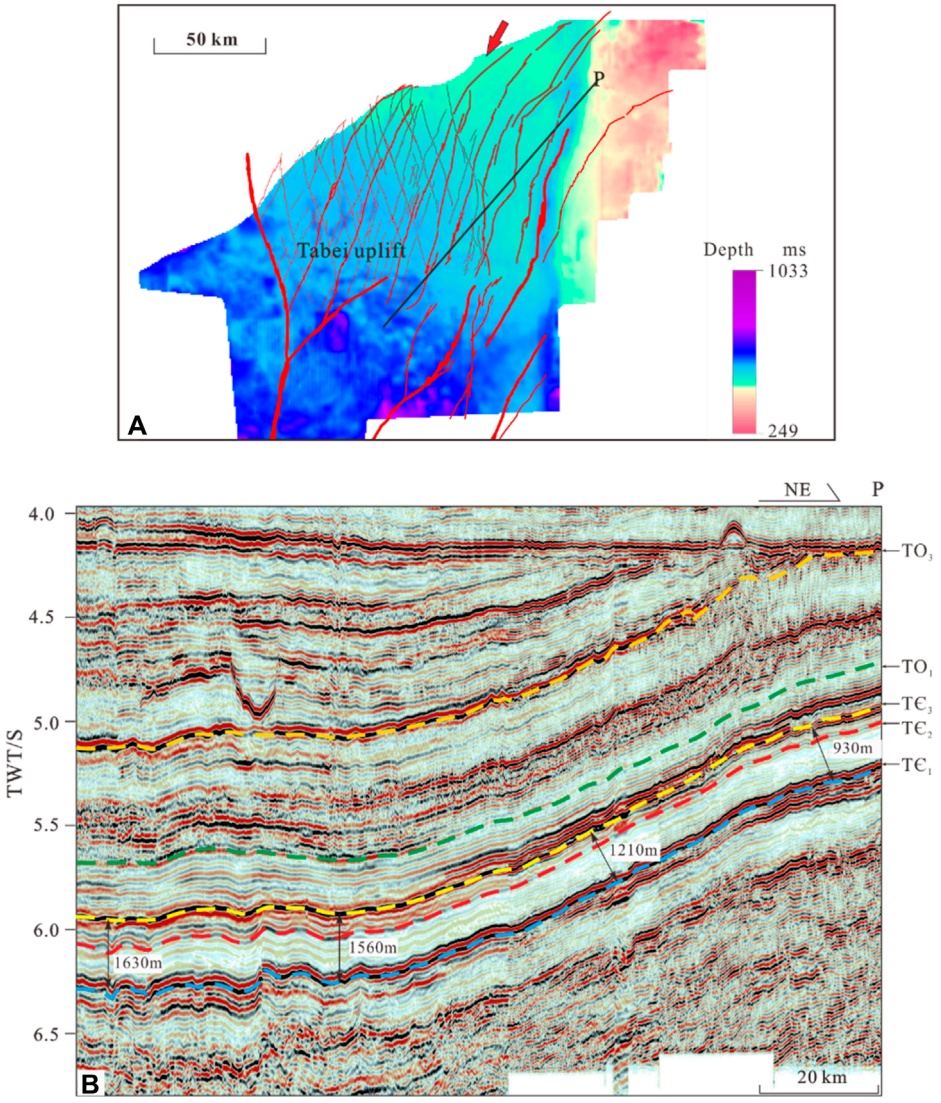

FIGURE 9
(A) The map of paleotectonic restoration of the Tabei Uplift of $T\epsilon_1$ in the late Middle Cambrian and **(B)** the seismic profiles presenting the stratigraphic configuration.

result of reactivation of underlying strike-slip faults. Growth strata within the deformation zone, present from the Silurian to the Carboniferous (Figures 7C, D), were influenced by the activity of normal faults, indicating that these faults were initiated in the Silurian and continued to be active through the Carboniferous.

6 Discussion

6.1 Features of the tectonic stress field in the Early Paleozoic

Researchers have extensively studied the evolving histories of the orogenic belts around the Tarim Basin, as it significantly affects the tectonic stress field in the basin. Most authors believe the basin was under a passive continental margin with an extensional tectonic stress field from the Cambrian to the Early Ordovician after the breakup of the Rodinia supercontinent (Jia, 1997; Wang, 2004). From the Middle to Late Ordovician, the ancient Kunlun and North Altyn Ocean subducted successively (Zhang et al., 2002; Wang, 2004; Li et al., 2009), and the basin was under an intensive compressive stress field in the NS direction. This subduction brought about the formation of the Tabei and Tazhong Uplifts with an EW orientation. The distribution patterns of unconformities were studied, which correlated well with the regional tectonic evolution studies (He et al., 2011; Lin et al., 2012; He et al., 2016). Nevertheless, research on the tectonic stress field patterns in the Tabei Uplift is insufficient, especially in the Early Paleozoic.

The bottom of the Lower Cambrian ($T\epsilon_1$) was selected, which was relatively stable and seldom affected by later denudation. According to the thickness of residual strata, the map of paleotectonic restoration of $T\epsilon_1$ during tectonic evolution were

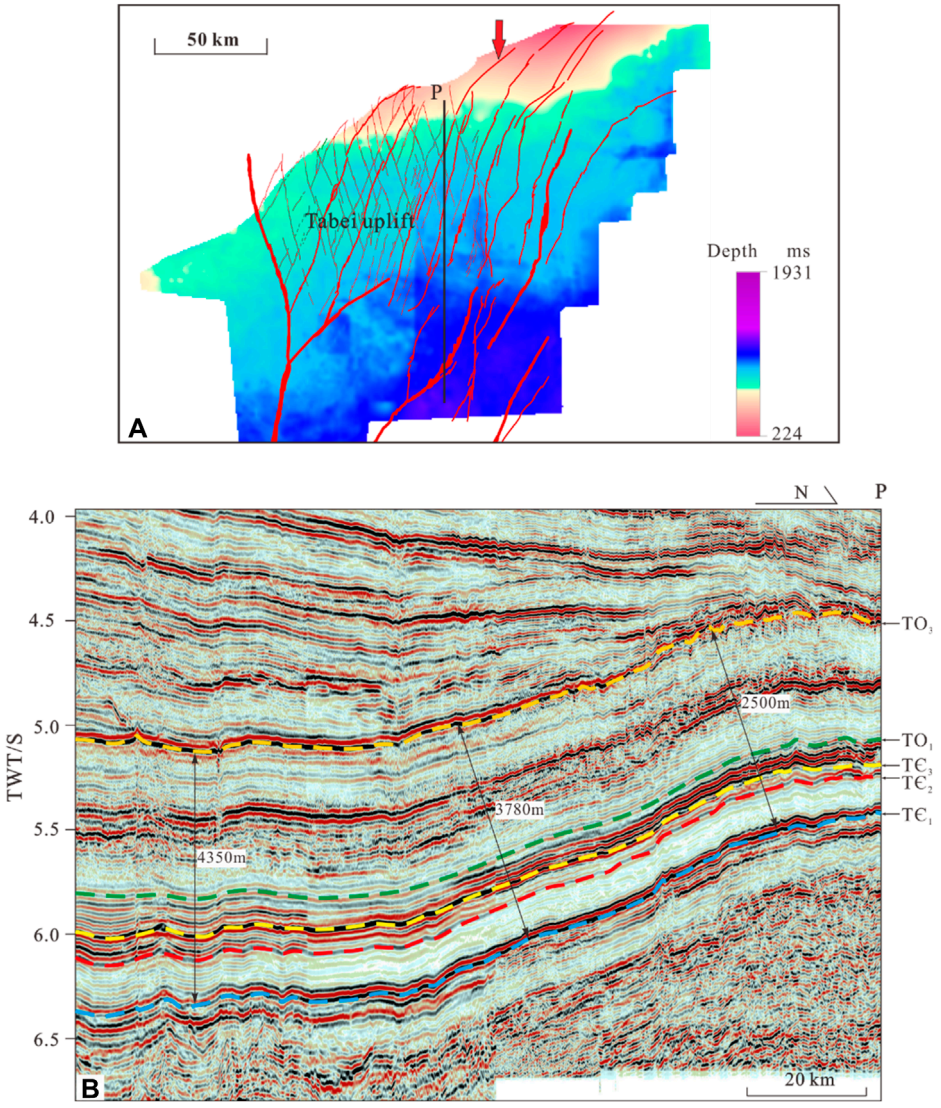

FIGURE 10
(A) The map of paleotectonic restoration of the Tabei Uplift of Tϵ_1 in the late Middle Ordovician and **(B)** the seismic profiles presenting the stratigraphic configuration.

restored, including the late of Early Cambrian (Figure 8A), the late of Middle Cambrian (Figure 9A), and the late of Middle Ordovician (Figure 10A).

The map of paleotectonic restoration comprises most regions of the Tabei and Manxi Low Uplifts according to the 3D seismic data provided by the CNPC. In the late of Early Cambrian, the paleotectonic map displayed high uplifts in the east, and most areas of the Tabei Uplift were in a depression, whereas the depression structure was not uniform. Some NW and NE-trending grooves developed and arranged linearly (Figure 8A) in the middle of the Tabei Uplift, reflecting the structural characteristics of the basement, correlating well with the trending of the two sets of strike-slip faults. On the seismic section, the structural patterns of the Precambrian rift are clear and affect the deposition of the overlying Lower Cambrian strata (Figure 8B). In the late of Middle Cambrian, the paleotectonic map exhibits a similar overall structural pattern as the late of Early Cambrian; however, the upheaval of the northeastern part of the Tabei Uplift occurred, and the sags in the Manxi Low Uplift oriented NW (Figure 9A), implying the direction of compressive stresses derived from the NE–SW in the north. The seismic profile shows that the strata thickness gradually decreases from the southwest to the northeast (Figure 9B). In the late of Middle Ordovician, the paleotectonic map feature changed dramatically. The overall structure framework was high in the north due to the considerable upheaval of the northern Tabei Uplift (Figure 10A), indicating that the direction of compressive stress transferred from north to south. The seismic profile shows that the thickness of the strata gradually thins from south to north (Figure 10B). Furthermore, the unconformity features in the Tarim Basin, developed from the Silurian to the Permian, have been systemically documented (Lin et al., 2012; He et al., 2016). The direction of compressive stress, from the

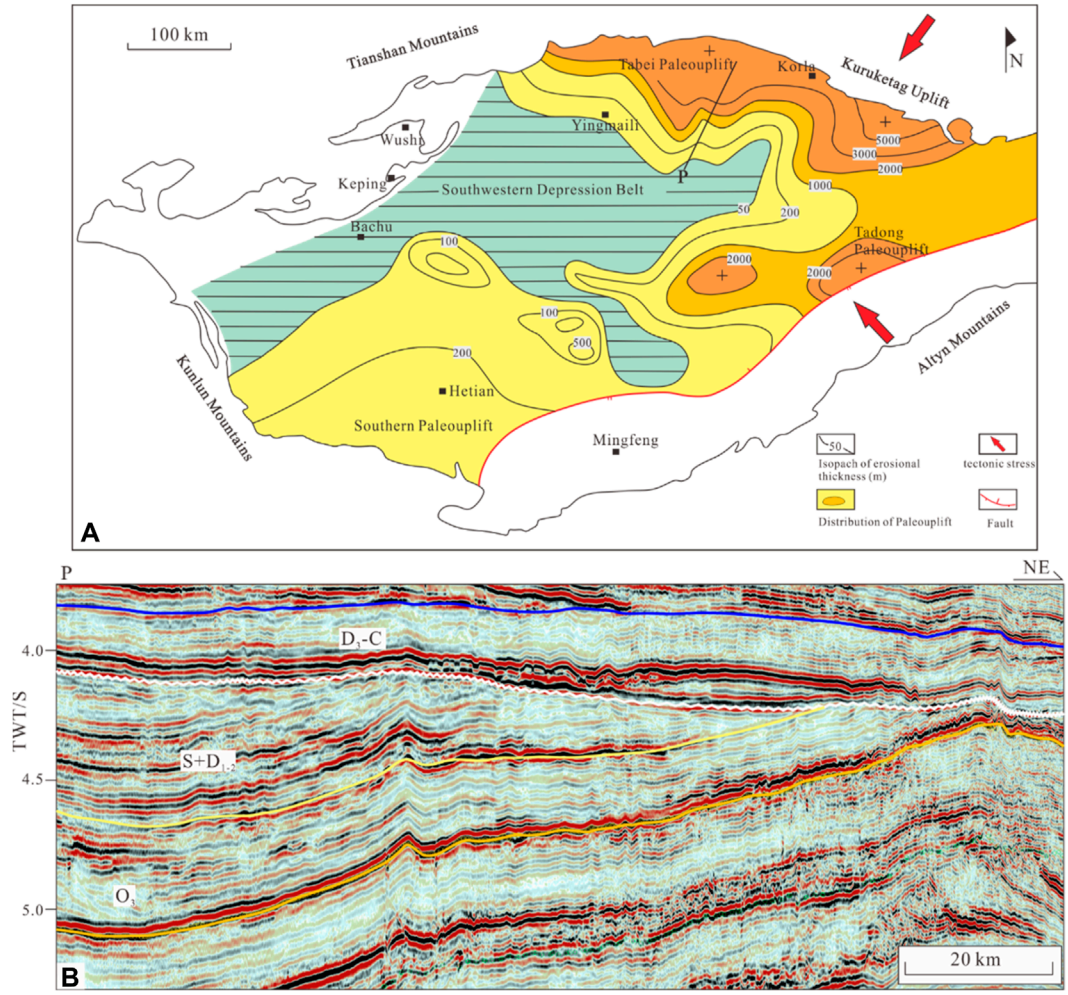

FIGURE 11
(A) The erosion thickness distribution of unconformity in the Devonian and the prediction of tectonic stress [modified from Lin et al. (2012), He et al. (2016)] and **(B)** seismic profile of the Devonian strata denudation in the Tabei Uplift.

Silurian to the Carboniferous, was demonstrated by patterns of erosion thickness (Figure 11A). The profile characteristics show that the large unconformity is widely developed in the Devonian (Figure 11B). The compressive stress primarily comes from the northeast and southeast (Figure 11A), corresponding to the closure of the south Tianshan and Altyn Oceans (Lin et al., 2012).

6.2 The formation mechanism of X-shaped faults in the Tabei Uplift

Numerous studies have been conducted to study the timing and formation mechanism of the X-shaped faults due to the significant hydrocarbon exploration findings along the strike-slip faults in the Tabei Uplift and the unique phenomena of small-angle X-type faults. Most authors consider the overall pattern of fault system controlled by a pure shear model, while the features of each fault correlate with the simple shear model. The faults were initiated in the Late Ordovician and developed a two-stage evolution (Wu et al., 2018; Deng et al., 2019; Ma et al., 2019; Wu et al., 2020b). However, debates exist about the controlling factors for the deviation of the dihedral angles of conjugate faults. Some authors propose that the lithology might significantly influence the dihedral angles of conjugate faults (Deng et al., 2018; Deng et al., 2019) because the internal friction coefficient varies with different lithologies. Besides, some scholars propose that fault reactivation and major fault orientation is a controlling factor for dihedral angles in the Tabei Uplift; the NW-trending faults significantly influence the dihedral angles (Wu et al., 2018; Wu et al., 2020a). Nevertheless, few studies have been conducted on the effects of preexisting basement structures on developing the strike-slip fault system in the Tabei Uplift.

Structure evolution and fault formation mechanisms in the Tabei Uplift were postulated in the study based on comprehensive interpretations of fault geometry features, analysis of tectonic stress field patterns, and features of the preexisting basement structures in the basin. The Precambrian normal faults in basement were detected on cross-sections from high-quality seismic data (Figures 3, 6, 8) (Neng et al., 2016; Yi et al., 2020; Chen et al., 2022). The map of paleotectonic restoration (Figure 7A) of the Lower Cambrian

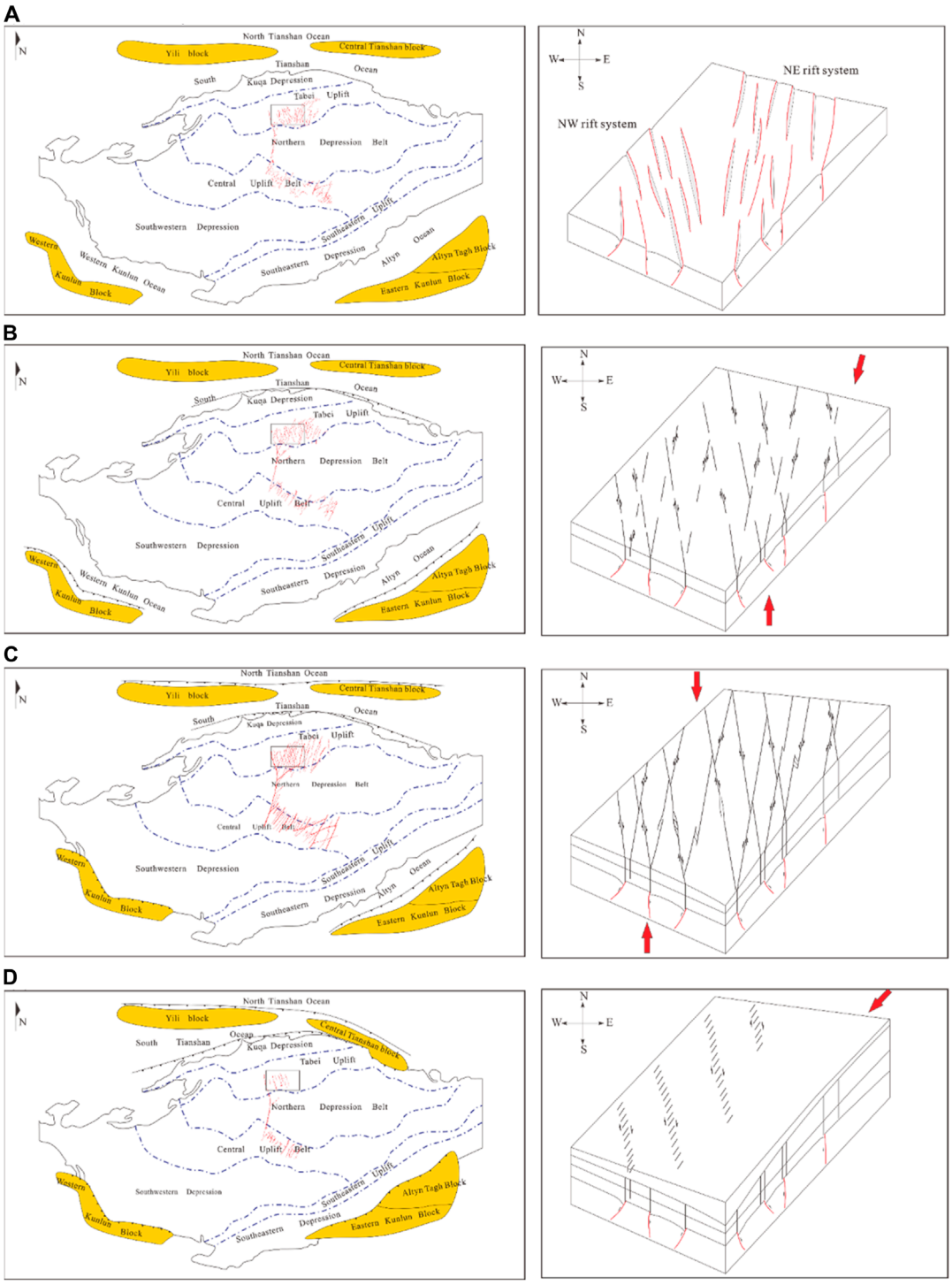

FIGURE 12
Evolution model of the surrounding blocks and the strike-slip fault system in the Tabei Uplift: **(A)** fault evolution in the Precambrian–Early Cambrian, **(B)** fault evolution in the Middle–Late Cambrian, **(C)** fault evolution in the Middle–Late Ordovician, **(D)** fault evolution in the Silurian–Carboniferous.

($T\epsilon_1$) at the late of Early Cambrian revealed that the rifts developed in the Tabei Uplift, distributed in the NW and NE directions (Figures 8A, B). This result correlates well with the trending of strike-slip faults, demonstrating that basement formations might significantly influence the Tabei Uplift's strike-slip fault evolution.

Following the breaking of the Rodinia supercontinent, the paleo ocean formed around the Tarim Block, and the basin was in a passive continental margin environment under an extensional setting from the Precambrian to the Early Ordovician. But there are still some uncertainties in the activity of orogenic belts around the

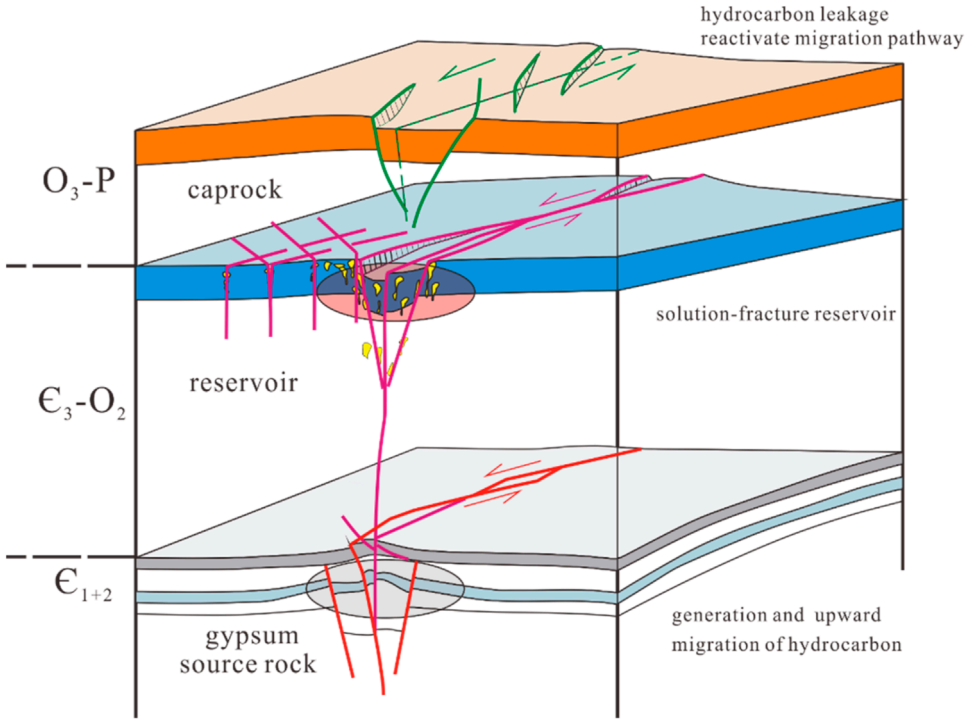

FIGURE 13
The simplified model for strike-slip fault controlling hydrocarbon accumulation.

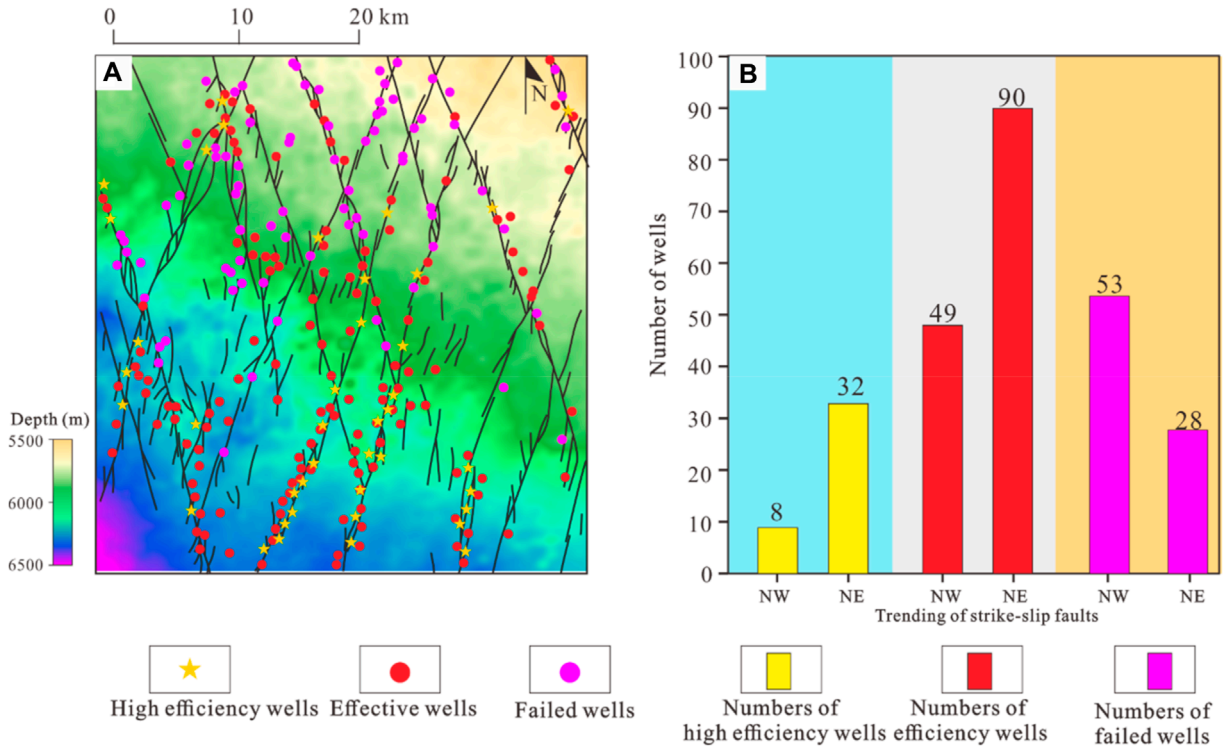

FIGURE 14
(A) The distribution of high-efficiency wells, effective wells and failed wells in Tabei Uplift (see location in Figure 1B). The basemap is the topographic map of the bottom of the Upper Ordovician in Tabei Uplift.; **(B)** The types of wells and the number of corresponding wells on the NE and NW Trending faults.

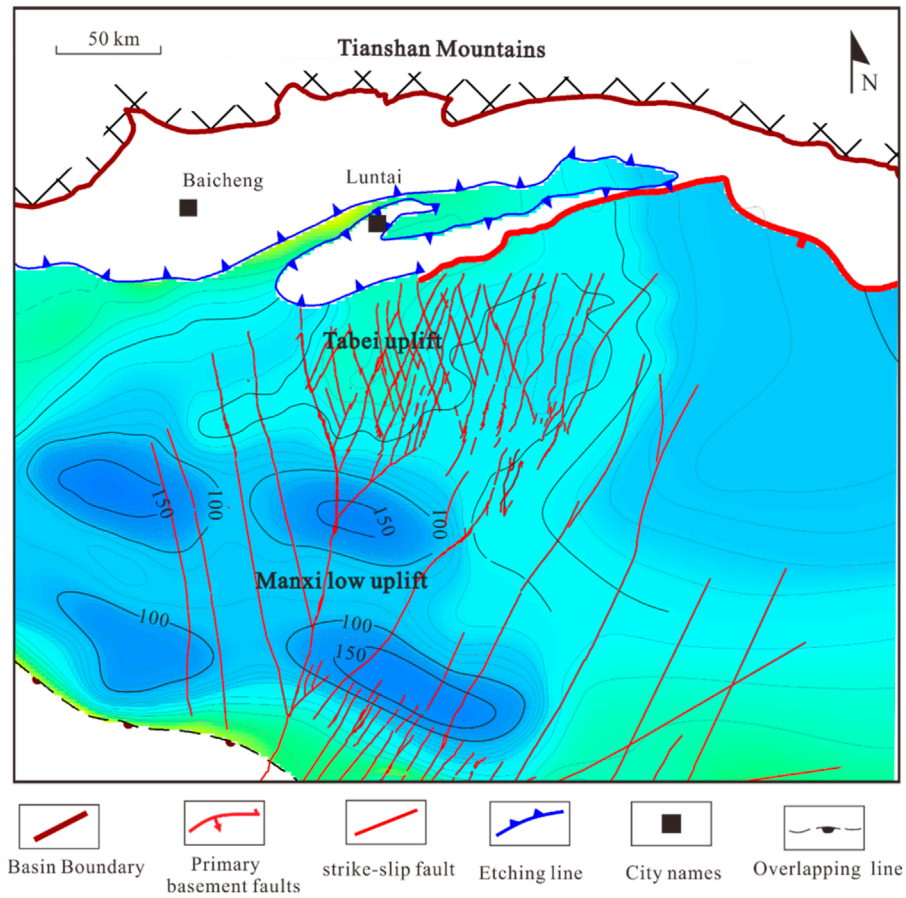

FIGURE 15
Distribution of source rocks of the Lower Cambrian Yuertus Formation around the Tabei Uplift.

basin in the Cambrian (Li et al., 2013; Wan et al., 2018). The latest researches proposed that at the end of the Middle Cambrian, the Proto-Tethys Ocean and the Paleo-Asian Ocean initially subducted (Xu et al., 2011; Ge et al., 2014; Han et al., 2015). The West Kunlun and Altyn Oceans gradually subducted in the south (Xiao et al., 2003; Liu et al., 2014), and the south Tianshan Ocean subducted southward in the north, resulting localized compressive–reverse movements occurred in the Middle–Late Cambrian (Gao and Fan, 2014). During the Middle to Late Cambrian, the Tabei Uplift experienced compressional tectonic stress from the northeast and south. This stress reactivated the basement rift systems, leading to the formation of NW- and NE-trending strike-slip faults. The angle between these two sets of rift systems is approximately 40° (Figure 8A), which resulted the formation of X-shaped fault system with small dihedral angles (Figures 12A, B).

Compressive stress emerged in the central Tarim Basin from the Middle to Late Ordovician due to the closure of the Ancient Kunlun and Altyn Oceans (Zhang et al., 2002; Li et al., 2009), the north Tianshan Ocean subduction towards the Central Tianshan microcontinent (Jia and Wei, 2002; Gao and Fan, 2014) and the continuous southward subduction of the south Tianshan Ocean (Han et al., 2015; Han et al., 2016). The Tabei Uplift was under a compressive tectonic stress field in N–S direction (Figure 10A). The Tabei Uplift was lifted and tilted southward during the period, verified by the thickness of the Upper Ordovician in the cross-section (Figure 10B). Under the compressive stress, the strike-slip faults were reactivated with a more significant deformation magnitude than previous stages (Figure 12C), punctured upward based on the underlying fault system, presented flower structures on the cross-section, and displayed linear segments with subordinate faults forming various patterns on the map view. The horsetail splay occurred at the south tip of the strike-slip faults (Figure 5C), indicating that the faults propagated from the north to the south and the compressive stress from the north was the dominant dynamic source of the Tabei Uplift.

The Tarim and Central Tianshan–Yining Blocks collided throughout the Silurian to the Carboniferous, and the South Tianshan Ocean gradually closed at the Carboniferous with a scissor-like form from east to west (Gao et al., 1998; Gao et al., 2006; Gao et al., 2009; Gao and Fan, 2014). The en-echelon normal faults formed within the period and most exhibit NE-trending with left-stepping in a NW linear arrangement parallel to the underlying strike-slip faults, interpreted as the tensional fracture from the progressive dextral movement of the NW-trending faults (Figure 12D). Moreover, the direction of compressive stress is indicated by the strike of en-echelon

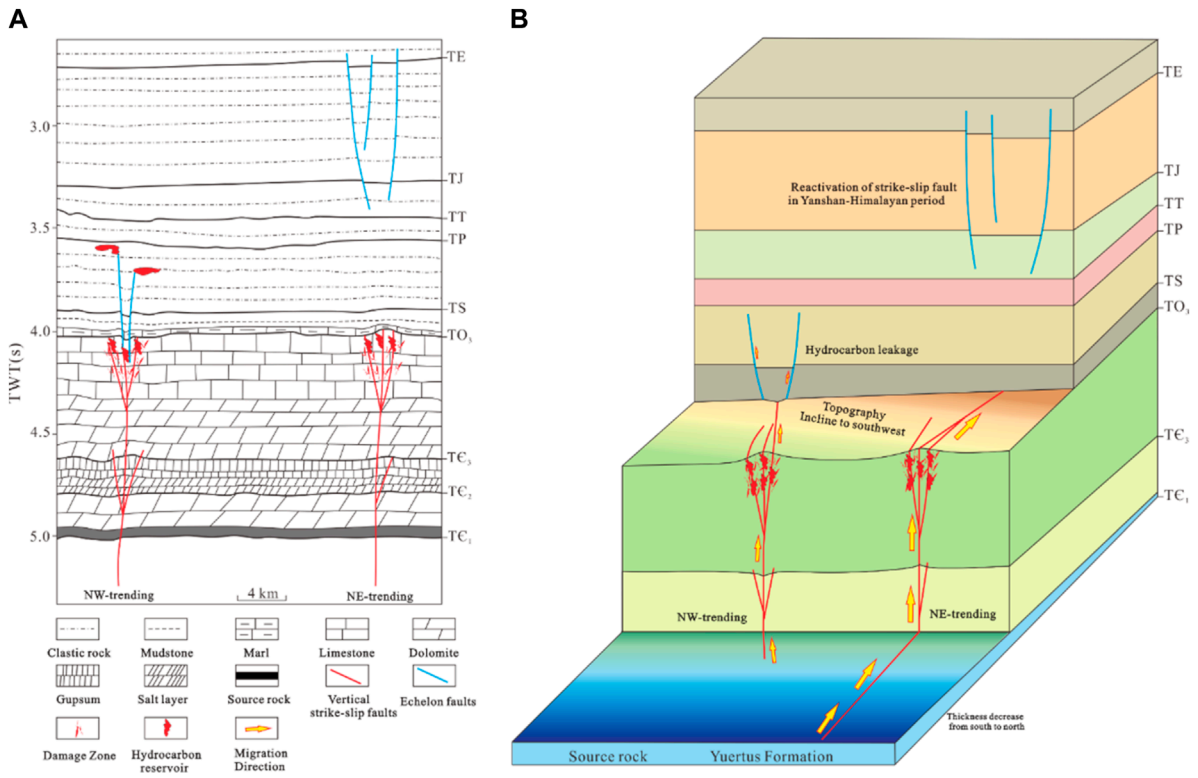

FIGURE 16
(A) Reservoir modeling and **(B)** the model of hydrocarbon differential enrichment in the Tabei Uplift.

normal faults unveils the tectonic stress field was under a NE–SW compressional stress, consistent with the unconformity distribution characteristics (Figure 11).

6.3 Factors controlling the hydrocarbon accumulation process

Significant hydrocarbon discoveries in the ultra-deep (>5,000 m) Paleozoic carbonate rocks were achieved around the Manjiaer depression. Most petroliferous wells were drilled within 1 km from the strike-slip fault (Wang et al., 2020; Tian et al., 2021; Wang et al., 2021). Many researchers have extensively studied the controlling factors of hydrocarbon accumulation. Most agreed that the Yuertusi Formation is the dominant source rock (Zhu et al., 2016; Wang et al., 2021; Zhu et al., 2022), developed in the Lower Cambrian, and the major hydrocarbon generating periods include the Late Caledonian, the Late Hercynian, and the Himalayan (Wang et al., 2020). Furthermore, the geometric patterns of strike-slip faults considerably influence the accumulation of hydrocarbons, influencing the development of reservoirs, including fractures and caves related to erosion (Deng et al., 2018; Wang et al., 2020; Deng et al., 2022). However, the role of layered deformation structure of strike-slip fault in hydrocarbon accumulation process remains unclear and why strike-slip faults in the Tabei Uplift are significantly hydrocarbon-enriched in various directions still controversial.

Based on detailed interpretations, three distinct deformation layers can be identified, each playing a different role in hydrocarbon accumulation and together constituting an independent petroleum system (Figure 13). The deep layer (below the $T\epsilon_3$) comprises Yuertusi Formation, which generates oil and gas, and the Middle Cambrian, a thick layer of salt and gypsum, which significantly influences the upward migration of hydrocarbon. The middle layer ($T\epsilon_3$–TO_3) developed a solution-fracture reservoir, mostly distributed in the Yinshan and Yijianfang Formations. The shallow layer (TO_3–TP) comprises thick mudstones and functions as caprock controlling the preservation of hydrocarbons. The evolutions of strike-slip faults correspond to the vertical deformation layers. The Middle-Late Cambrian deformation cut through the thick salt and gypsum layer and provided the channels for hydrocarbon upward migration in subsequent periods. The Middle-Late Ordovician deformation generated a damage zone in the carbonate strata along the faults, provided meteoric water and hydrothermal fluids paths to penetrate and erode, and formed a fracture-solution reservoir. The en-echelon faults, which have been active from the Silurian to the Carboniferous, resulted from the underlying strike-slip fault system being reactivated. They might cut through the caprock and cause hydrocarbon leaks. In addition, the reactivation of strike-slip faults might enhance the hydrocarbon upward migration and restore the migration efficiency of sealed fault panels from the Cambrian source rock to the Ordovician carbonate reservoir, especially during the accumulation periods.

The Tabei Uplift's reservoir development is in good condition (Ma et al., 2019; Wu et al., 2020a), and the carbonate fracture-cave

reservoir is developed along the strike-slip fault damage zone. The NW-trending fault activity is stronger, and the internal reservoir is significantly better. However, most high-efficiency wells are found in the NE-trending strike-slip faults (Chen et al., 2023), whereas NW-trending strike-slip faults offer inferior conditions for hydrocarbon enrichment (Figures 14A, B).

NW- and NE-trending strike-slip faults have suitable conditions for reservoir development (Chen et al., 2023). The distribution characteristics of wells show that the number of efficient wells and effective wells in the south is much more than that in the north, while more failed wells are distributed in the north (Figure 14A). The difference in fault-controlled hydrocarbon enrichment might be affected by the distribution characteristics of source rocks and hydrocarbon migration conditions (Figures 15, 16).

Accordingly, the sedimentary center of the Yuertus Formation is primarily in the Manxi Low Uplift (Tian et al., 2021; Wang et al., 2021), gradually thinning to the Tabei Uplift (Figure 15). The hydrocarbon generation center is in the Manxi Low Uplift and serves as a source for hydrocarbon migration to the paleo uplift. The bottom of Upper Ordovcian in the Tabei Uplift is inclined to the southwest (Figure 14A) (Ning et al., 2020), and the NE direction becomes dominant for hydrocarbon migration due to the influence of potential energy. It is advantageous for hydrocarbon migration along the NE direction that the large strike-slip faults through the Tabei and Manxi Low Uplifts are NE-trending (Figure 1B). Furthermore, the en-echelon normal faults, which developed along the NW-trending strike-slip faults from the Silurian to the Carboniferous, may have cut through the caprock, leading to hydrocarbon leakage (Figures 4D, 16). Also, the NE-trending fault fully accepted the hydrocarbon filling due to reactivation during the Yanshan and Himalayan periods (Deng et al., 2018, 2022), which corresponds to the stages of hydrocarbon charging (Figure 16).

7 Conclusion

1) The Tabei Uplift has two sets of extensively developed X-type intersecting strike-slip faults that can be separated into three structural deformation layers and exhibit typical layered differential deformation characteristics: rifts, weak strike-slip deformation, and salt tectonics are developed in the deep structural layer; strong, strike-slip deformation and karst-dissolution structures are primarily developed in the middle structural layer; and the echelon normal faults are developed in the shallow structural layer.
2) Strike-slip fault tectonic evolution can be classified into three stages, and the formation of small-angled X-type strike-slip is influenced by basement rift significantly. Two groups of small-angled X-type strike-slip faults formed along the two sets of basement rift systems under the effect of localized compressive stress in the Middle–Late Cambrian. The strike-slip fault was extensively deformed during the Middle–Late Ordovician when the periphery orogenic belts were active, and it was inherited and developed along the underling fault system. Strike-slip faults were reactivated due to the closing of the South Tianshan Ocean during the Silurian–Carboniferous and echelon normal faults developed in the shallow structural layer.
3) The layered deformation structure of strike-slip faults impacts hydrocarbon accumulation as an independent petroleum system. The deep structural layer influences the generation of oil and gas and its upward migration. The middle structural layer controls the reservoir formation of the karst-dissolution; the shallow layer affects the preservation of hydrocarbons and the opening of migration channels. NE-trending faults have a higher level of hydrocarbon enrichment than NW-trending strike-slip faults, influenced by the distribution of source rocks and large-scale faults, topography of the Tabei Uplift, and the features of fault reactivation.

Data availability statement

The original contributions presented in the study are included in the article/supplementary material, further inquiries can be directed to the corresponding author.

Author contributions

XS: Writing–original draft. SC: Writing–review and editing. YZ: Conceptualization, Writing–original draft. ZX: Data curation, Writing–original draft. XL: Methodology, Writing–review and editing. MY: Supervision, Writing–review and editing. MZ: Validation, Writing–review and editing. XS: Resources, Writing–review and editing.

Funding

The authors declare that financial support was received for the research, authorship, and/or publication of this article. This study was financially supported by the National Natural Sciences Foundation of China (Grant No. U21B2062).

Conflict of interest

Authors YZ, ZX, MZ, and XS were employed by PetroChina Tarim Oilfield Company.

The remaining authors declare that the research was conducted in the absence of any commercial or financial relationships that could be construed as a potential conflict of interest.

Publisher's note

References

Anderson, B. E. M. (1951). The dynamics offaulting. *Eainbwrgh, Vnited Kingd. Oliverand Boyd*, 1–206.

Chen, H. L., Yang, S. F., Wang, Q. H., Luo, J. C., Jia, C. Z., Wei, G. Q., et al. (2006). Sedimentary response to the early-MidPermian basaltic magmatism in the Tarim plate. *Geol. China* 33 (03), 545–552. (in Chinese with English abstract). doi:10.3969/j.issn.1000-3657.2006.03.010

Chen, L. X., Jia, C. Z., Jiang, Z. X., Su, Z., Yang, M. C., Yang, B., et al. (2023). Oil enrichment model and main controlling factors of carbonate reservoirs in Halahatang area, Tarim Basin. *Acta Pet. Sin.* 44 (06), 948–961

Chen, S., Zhang, Y. T., Xie, Z., Song, X. G., and Liang, X. X. (2024). Multi-stages of paleozoic deformation of the fault system in the Tazhong uplift, Tarim Basin, NW China: implications for hydrocarbon accumulation. *J. Asian Earth Sci.* 265, 106086. doi:10.1016/j.jseaes.2024.106086

Chen, Y. Q., Wang, X. X., He, H., and Yi, Y. (2022). Evolution of uplift and depression framework of Tarim craton in nanhua-cambrian. *China Pet. Explor.* 27 (4), 30–46. (in Chinese with English abstract). doi:10.3969/j.issn.1672-7703.2022.04.003

Christie-Blick, N., and Biddle, K. T. (1985). Deformation and basin formation along strikeslip fault. *Soc. Econ. Paleontol. Mineral. Spec. Pub.* 37, 1–34. doi:10.2110/pec.85.37.0001

Deng, S., Li, H. L., Zhang, Z. P., Wu, X., and Zhang, J. B. (2018). Characteristics of differential activities in major strike-slip fault zones and their control on hydrocarbon enrichment in Shunbei area and its surroundings, Tarim Basin. *Oil. Gas. Geol.* 39 (05), 978–888. (in Chinese with English abstract). doi:10.11743/ogg20180503

Deng, S., Li, H. L., Zhang, Z. P., Zhang, J. B., and Yang, X. (2019). Structural characterization of intracratonic strike-slip faults in the central Tarim Basin. *AAPG Bull.* 103, 109–137. doi:10.1306/06071817354

Deng, S., Liu, Y. Q., Liu, J., Han, J., Wang, B., and Zhao, R. (2021). Structural styles and evolution models of intracratonic strike-slip faults and the implications for reservoir exploration and appraisal: a case study of the Shunbei area, Tarim Basin. *Geotect. Metallog.* 45 (6), 1111–1126. (in Chinese with English abstract). doi:10.16539/j.ddgzyckx.2020.05.015

Deng, S., Zhao, R., Kong, Q., Li, Y., and Li, B. (2022). Two distinct Strike-Slip Fault networks in the Shunbei area and its surroundings, Tarim Basin: hydrocarbon accumulation, distribution, and controlling factors. *AAPG Bull.* 106 (1), 77–102. doi:10.1306/07202119113

Fan, C. H., Nie, S., Li, H., Radwan, A. E., Pan, Q. C., Shi, X. C., et al. (2024). Quantitative prediction and spatial analysis of structural fractures in deep shale gas reservoirs within complex structural zones: a case study of the Longmaxi Formation in the Luzhou area, southern Sichuan Basin, China. *J. Asian Earth Sci.* 263, 106025. doi:10.1016/j.jseaes.2024.106025

Gao, J., Li, M. S., Xiao, X. C., Tang, Y., and He, G. (1998). Paleozoic tectonic evolution of the Tianshan Orogen, northwestern China. *Tectonophysics* 287 (1-4), 213–231. doi:10.1016/s0040-1951(97)00211-4

Gao, J., Long, L. L., Klemd, R., Qian, Q., Liu, D. Y., Xiong, X. M., et al. (2009). Tectonic evolution of the South Tianshan orogen and adjacent regions, NW China: geochemical and age constraints of granitoid rocks. *Int. J. Earth Sci.* 98, 1221–1238. doi:10.1007/s00531-008-0370-8

Gao, J., Long, L. L., Qian, Q., Huang, D. Z., Su, W., and Reiner, K. (2006). South tianshan: a late paleozoic or a triassic orogen? *Acta Pet. Sin.* 22 (5), 1049–1061. doi:10.3969/j.issn.1000-0569.2006.05.001

Gao, Z. Q., and Fan, T. L. (2014). Intra-platform tectono-sedimentary response to geodynamic transition along the margin of the Tarim Basin, NW China. *J. Asian Earth Sci.* 96, 178–193. doi:10.1016/j.jseaes.2014.08.023

Ge, R., Zhu, W., Wilde, S. A., He, J., Cui, X., Wang, X., et al. (2014). Neoproterozoic to Paleozoic long-lived accretionary orogeny in the northern Tarim Craton. *Tectonics* 33 (03), 302–329. doi:10.1002/2013tc003501

Graham, S. A., Hitzman, M., McCloy, C., Turner, R., and Ward, R. (1984). Basin evolution during change from convergent to transform continental margin in central California. *AAPG Bull.* 68 (3), 223–249. doi:10.1306/ad460a03-16f7-11d7-8645000102c1865d

Han, X. Y., Deng, S., Tang, L. J., and Cao, Z. C. (2017). Geometry, kinematics and displacement characteristics of strike-slip faults in the northern slope of Tazhong uplift in Tarim Basin: a study based on 3D seismic data. *Pet. Geol.* 88, 410–427. doi:10.1016/j.marpetgeo.2017.08.033

Han, Y., Zhao, G., Cawood, P. A., Sun, M., Eizenhofer, P. R., Hou, W., et al. (2016). Tarim and North China cratons linked to northern Gondwana through switching accretionary tectonics and collisional orogenesis. *Geology* 44 (02), 95–98. doi:10.1130/g37399.1

Han, Y., Zhao, G., Sun, M., Eizenhofer, P. R., Hou, W., Zhang, X., et al. (2015). Paleozoic accretionary orogenesis in the Paleo-Asian Ocean: insights from detrital zircons from silurian to carboniferous strata at the northwestern margin of the Tarim craton. *Tectonics* 34 (02), 334–351. doi:10.1002/2014tc003668

Harding, T. P. (1974). Petroleum traps associated with wrench faults. *AAPG Bull.* 58 (7), 1290–1304. doi:10.1306/83d91669-16c7-11d7-8645000102c1865d

Harding, T. P. (1985). Seismic characteristics and identification of negative flower structures, positive flower structures, and positive structural inversion. *AAPG Bull.* 69 (4), 582–600. doi:10.1306/ad462538-16f7-11d7-8645000102c1865d

He, B. Z., Jiao, C. L., Xu, Z. Q., Cai, Z. H., Zhang, J. X., Liu, S. L., et al. (2016). The paleotectonic and paleogeography reconstructions of the Tarim Basin and its adjacent areas (NW China) during the late Early and Middle Paleozoic. *Gondwana Res.* 30, 191–206. doi:10.1016/j.gr.2015.09.011

He, B. Z., Xu, Z. Q., Jiao, C. L., Li, H. B., and Cai, Z. H. (2011). Tectonic unconformities and their forming: implication for hydrocarbon accumulations in Tarim basin. *Acta Pet. Sin.* 27 (01), 253–265.

He, D. F., Jia, C. Z., Li, D. S., Zhang, C. J., Meng, Q. R., and Shi, X. (2005). Formation and evolution of polycyclic superimposed Tarim Basin. Oil. *Gas. Geol.* 26 (01), 64–77. (in Chinese with English abstract). doi:10.3321/j.issn:0253-9985.2005.01.010

He, D. F., Zhou, X. Y., Zhang, C. J., Yang, W. J., and Shi, X. (2006). Characteristics of geologic framework of multicycle superimposed basin in Tarim Basin. *Pet. Geol.* 11 (1), 31–41. (in Chinese with English abstract). doi:10.3969/j.issn.1672-7703.2006.01.006

Ismat, Z. (2015). What can the dihedral angle of conjugate-faults tell us? *Jounral Structral Geol.* 73, 97–113. doi:10.1016/j.jsg.2015.02.008

Jia, C. Z. (1997). *Tectonic characteristics and petroleum, Tarim Basin. China. Pet.* Ind. Press, 1–120. (in Chinese with English abstract).

Jia, C. Z., Ma, D. B., Yuan, J. Y., Wei, G. Q., Yang, M., Yan, L., et al. (2021). Structural characteristics, formation and evolution and genetic mechanisms of strike–slip faults in the Tarim Basin. *Nat. Gas. Ind.* 41 (08), 81–91. (in Chinese with English abstract). doi:10.3787/j.issn.1000-0976.2021.08.008

Jia, C. Z., and Wei, G. Q. (2002). Structural characteristics and petroliferous features of Tarim Basin. *Chin. Sci. Bull.* 47, 1–11. doi:10.1007/bf02902812

Jiao, F. Z. (2018). Significance and prospect of ultra-deep carbonate fault-karst reservoir in Shunbei area, Tarim Basin. *Oil. Gas. Geol.* 39 (02), 207–216. (in Chinese with English abstract). doi:10.11743/ogg20180201

Li, C. X., Jia, C. Z., Li, B., Yang, G., Yang, H. J., Luo, C. S., et al. (2009). Distribution and tectonic evolution of the Paleozoic fault system, the north slope of Tazhong uplift, Tarim Basin. *Acta Geol. Sin.* 83 (8), 1065–1073. (in Chinese with English abstract). doi:10.3321/j.issn:0001-5717.2009.08.002

Li, C. X., Wang, X. F., Li, B. L., and He, D. F. (2013). Paleozoic fault systems of the Tazhong uplift, Tarim Basin, China. *AAPG Bull.* 39, 48–58. doi:10.1016/j.marpetgeo.2012.09.010

Li, D. S., Liang, D. G., Jia, C. Z., Wang, G., Wu, Q. Z., and He, D. F. (1996). Hydrocarbon accumulation in the Tarim Basin, China. *AAPG Bull.* 80 (10), 1587–1603. doi:10.1306/64eda0be-1724-11d7-8645000102c1865d

Li, D. X., Yang, S. F., Chen, H. L., Cheng, X. G., Li, K., Jin, X. L., et al. (2014). Late carboniferous crustal uplift of the Tarim plate and its constraints on the evolution of the early permian Tarim large igneous province. *Lithos* 204, 36–46. doi:10.1016/j.lithos.2014.05.023

Li, H., Tang, H. M., Qin, Q. R., Zhou, J. L., Qin, Z. J., Fan, C. H., et al. (2019). Characteristics, formation periods and genetic mechanisms of tectonic fractures in the tight gas sandstones reservoir: a case study of Xujiahe Formation in YB area, Sichuan Basin, China. *J. Petroleum Sci. Eng.* 178, 723–735. doi:10.1016/j.petrol.2019.04.007

Lin, C. S., Yang, H. J., Liu, J. Y., Rui, Z. F., Cai, Z. Z., and Zhu, Y. F. (2012). Distribution and erosion of the Paleozoic tectonic unconformities in the Tarim Basin, Northwest China: significance for the evolution of paleo-uplifts and tectonic geography during deformation. *J. Asian Earth Sci.* 46, 1–19. doi:10.1016/j.jseaes.2011.10.004

Liu, K. F., Wang, Y. H., Jiang, G. L., Zhang, S. M., and Zhang, K. X. (2014). Evolution of neoproterozoic-mesozoic sedimentary basin of West Kunlun area. *Earth Sci.* 39 (08), 987–999. (in Chinese with English abstract). doi:10.3799/dqkx.2014.090

Liu, Y., Suppe, J., Cao, Y. C., Hao, F., Liu, Y. D., Wang, X., et al. (2023). Linkage and formation of strike-slip faults in deep basins and the implications for petroleum accumulation: a case study from the Shunbei area of the Tarim Basin, China. *AAPG Bull.* 107 (02), 331–355. doi:10.1306/11142220110

Liu, Y. J., Neubauer, F., Genser, J., Ge, X. H., Takasu, A., Yuan, S. H., et al. (2007). Geochronology of the initiation and displacement of the Altyn strike-slip fault, western China. *J. Asian Earth Sci.* 29 (2-3), 243–252. doi:10.1016/j.jseaes.2006.03.002

Ma, D. B., Wu, G. H., Zhu, Y. F., Tao, X. W., Chen, L. X., Li, P. F., et al. (2019). Segmentation characteristics of deep strike slip faults in the Tarim Basin and its control on hydrocarbon enrichment: taking the Ordovician strike slip fault in the Halahatang Oilfield in the Tabeiarea as an example. *Earth Sci. Front.* 26 (1), 225–237. (in Chinese with English abstract). doi:10.13745/j.esf.sf.2019.1.10

Mandl, G. (2000). *Faulting in brittle rocks: an introduction to the mechanics of tectonic faults*. New York: Springer.

Mattern, F., and Schneider, W. (2000). Suturing of the proto-and paleo-tethys oceans in the western Kunlun (xinjiang, China). *J. Asian Earth Sci.* 18 (6), 637–650. doi:10.1016/s1367-9120(00)00011-0

Morley, C. K. (2014). Outcrop examples of soft-sediment deformation associated with normal fault terminations in deepwater, Eocene turbidites: a previously undescribed conjugate fault termination style? *Jounral Structral Geol.* 69, 189–208. doi:10.1016/j.jsg.2014.10.003

Nakajima, T., Maruyama, S., Uchiumi, S., Liou, J. G., Wang, X. Z., Xiao, X. C., et al. (1990). Evidence for late proterozoic subduction from 700-Myr-old blueschists in China. *Nature* 346 (6281), 263–265. doi:10.1038/346263a0

Neng, Y., Li, Y., Qi, J. F., Ma, X., Zuo, L., and Chen, P. (2022). Deformation styles and multi-stage evolution history of a large intraplate Strike-Slip Fault system in a paleozoic superimposed basin: a case study from the Tarim Basin, NW China. *Front. Earth Sci.* 10, 837354. doi:10.3389/feart.2022.837354

Neng, Y., Wu, G. H., Huang, S. Y., Zhang, X., and Cao, S. J. (2016). Formation stage and controlling factors of the paleo-uplifts in the Tarim Basin: a further discussion. *Nat. Gas. Ind.* 36 (04), 209–215. (in Chinese with English abstract). doi:10.1016/j.ngib.2016.05.005

Ning, C. Z., Hu, S. Y., Pan, W. Q., Yao, Z. X., Li, Y., and Yuan, W. F. (2020). Characterization of paleo-topography and karst caves in ordovician lianglitage formation, Halahatang oilfield, Tarim Basin. *Oil. Gas Geol* 41 (5), 985–995. (in Chinese with English abstract). doi:10.11743/ogg20200509

Ramadan, G., Jean-Marc, D., Catherin, D., Fadi, H. N., and John, E. C. (2014). Impact of Cenozoic strike-slip tectonics on the evolution of the northern Levant Basin (offshore Lebanon). *Tectonics* 33 (11), 2121–2142. doi:10.1002/2014tc003574

Ramsey, J. M., and Chester, F. M. (2004). Hybrid fracture and the transition from extension fracture to shear fracture. *Nature* 428 (6978), 63–66. doi:10.1038/nature02333

Romeo, I., Capote, R., and Anguita, F. (2005). Tectonic and kinematic study of a strike-slip zone along the southern margin of Central Ovda Regio, Venus: geodynamical implications for crustal plateaux formation and evolution. *Icarus* 175 (2), 320–334. doi:10.1016/j.icarus.2004.11.007

Shen, Z. Y., Neng, Y., Han, J., Huang, C., Zhu, X. X., Chen, P., et al. (2022). Structural styles and linkage evolution in the middle segment of a strike-slip fault: a case from the Tarim Basin, NW China. *J. Struct. Geol.* 157, 104558. doi:10.1016/j.jsg.2022.104558

Sun, Q. Q., Fan, T. L., Gao, Z. Q., Wu, J., Zhang, H. H., Jiang, Q., et al. (2021). New insights on the geometry and kinematics of the Shunbei 5 strike-slip fault in the central Tarim Basin, China. *Jounral Structral Geol.* 150, 104400. doi:10.1016/j.jsg.2021.104400

Swanson, M. T. (2005). Geometry and kinematics of adhesive wear in brittle strikeslip fault zones. *J. Struct. Geol.* 27, 871–887. doi:10.1016/j.jsg.2004.11.009

Tang, L. J. (1994). Evolution and tectonic patterns of Tarim Basin. *Earth Sci.* 19 (06), 742–754. doi:10.3321/j.issn:1000-2383.1994.06.006

Tian, J., Yang, H. J., Zhu, Y. F., Deng, X. L., Xie, Z., Zhang, Y. T., et al. (2021). Geological conditions for hydrocarbon accumulation and key technologies for exploration and development in Fuman oilfield, Tarim Basin. *Acta Pet. Sin.* 42 (08), 971–975. (in Chinese with English abstract). doi:10.7623/syxb202108001

Tondi, E., Cilona, A., Agosta, F., Aydin, A., Rustichelli, A., Renda, P., et al. (2012). Growth processes, dimensional parameters and scaling relationships of two conjugate sets of compactive shear bands in porous carbonate grainstones, Favignana Island, Italy. *J. Struct. Geol.* 37, 53–64. doi:10.1016/j.jsg.2012.02.003

Wan, B., Li, S., Xiao, W. J., and Windley, B. F. (2018). Where and when did the Paleo-Asian ocean form? *Precambrian Res.* 317, 241–252. doi:10.1016/j.precamres.2018.09.003

Wang, B., Zhao, Y. Q., He, S., Guo, X. W., Cao, Z. C., Deng, S., et al. (2020a). Hydrocarbon accumulation stages and their controlling factors in the northern Ordovician Shunbei 5 fault zone, Tarim Basin. *Oil Gas. Geol.* 41 (5), 965–974. (in Chinese with English abstract). doi:10.11743/ogg20200507

Wang, Q. H., Yang, H. J., Wang, R. J., Li, S. Y., Li, Y., Chang, L. J., et al. (2021). Discovery and exploration technology of fault-controlled large oil and gas fields of ultra-deep formation in strike slip fault zone in Tarim Basin. *China Pet. Explor.* 26 (4), 58–71. (in Chinese with English abstract). doi:10.3969/j.issn.1672-7703.2021.04.005

Wang, Z. H. (2004). Tectonic evolution of the western Kunlun orogenic belt, western China. *J. Asian Earth Sci.* 24 (2), 153–161. doi:10.1016/j.jseaes.2003.10.007

Wang, Z. Y., Gao, Z. Q., Fan, T. L., Shang, Y. X., Qi, L. X., and Yun, L. (2020b). Structural characterization and hydrocarbon prediction for the SB5M strike-slip fault zone in the Shuntuo Low Uplift, Tarim Basin. *Pet. Geol.* 117, 104418. doi:10.1016/j.marpetgeo.2020.104418

Wu, G. H., Kim, Y. S., Su, Z., Yang, P. F., Ma, D. B., and Zheng, D. M. (2020c). Segment interaction and linkage evolution in a conjugate strike-slip fault system from the Tarim Basin, NW China. *Pet. Geol.* 112, 104054. doi:10.1016/j.marpetgeo.2019.104054

Wu, G. H., Ma, B. S., Han, J. F., Guan, B. Z., Chen, X., Yang, P., et al. (2021). Origin and growth mechanisms of strike-slip faults in the central Tarim cratonic basin, NW China. *Develop* 48 (3), 595–607. doi:10.1016/s1876-3804(21)60048-4

Wu, G. H., Yang, S., Meert, J. G., Xiao, Y., Chen, Y. Q., Wang, Z. C., et al. (2020a). Two phases of paleoproterozoic orogenesis in the Tarim craton: implications for columbia assembly. *Gondwana Res.* 83, 201–216. doi:10.1016/j.gr.2020.02.009

Wu, G. H., Yuan, Y. J., Huang, S. Y., Thomas, M. V., Xiao, Y., Cai, Q., et al. (2018a). The dihedral angle and intersection processes of a conjugate Strike-Slip Fault system in the Tarim Basin, NW China. *ACTA Geol. SIN. Engl. Ed.* 92 (01), 74–88. doi:10.1111/1755-6724.13495

Wu, G. H., Zhao, K. Z., Qu, H. Z., Scarselli, N., Zhang, Y. T., Han, J. F., et al. (2020b). Permeability distribution and scaling in multi-stages carbonate damage zones: insight from strike-slip fault zones in the Tarim Basin, NW China. *Pet. Geol.* 114, 104208. doi:10.1016/j.marpetgeo.2019.104208

Wu, L., Guan, S. W., Zhang, S. C., Yang, H. J., Jin, J. Q., Zhang, X. D., et al. (2018b). Neoproterozoic stratigraphic framework of the Tarim craton in NW China: implications for rift evolution. *J. Asian Earth Sci.* 158, 240–252. doi:10.1016/j.jseaes.2018.03.003

Xiao, W. J., Fang, A. M., Li, J. L., Zhou, H., B, F. W., Yuan, C., et al. (2003). Structures and evolution of the multiple accretionary complexes, western Kunlun Orogenic belt (China). *Xinjiang Geol.* 21 (01), 31–36. (in Chinese with English abstract). doi:10.3969/j.issn.1000-8845.2003.01.005

Xu, X., Zuza, A. V., Yin, A., Lin, X. B., Chen, H. L., and Yang, S. F. (2021). Permian plume strengthened Tarim lithosphere controls the cenozoic deformation pattern of the himalayan-Tibetan orogen. *Geology* 49 (1), 96–100. doi:10.1130/g47961.1

Xu, Z. Q., Li, S. T., Zhang, J. X., Yang, J. S., He, B. Z., Li, H. B., et al. (2011). Paleo-Asian and Tethyan tectonic systems with docking the Tarim block. *Acta Petrol. Sin.* 27 (01), 1–22. (in Chinese with English abstract).

Yang, H. J., Wu, G. H., Han, J. F., and Su, Z. (2020). Structural analysis of strike-slip faults in the Tarim intracratonic basin. *Chin. J. Geol.* 55 (01), 1–16. (in Chinese with English abstract). doi:10.12017/dzkx.2020.001

Yang, S. F., Chen, H. L., Dong, C. W., Jia, C. Z., and Wang, Z. G. (1996). The discovery of permiansyenite inside Tarim Basin and its geodynamic significance. *Geochimica* 25, 121–128. (in Chinese with English abstract). doi:10.19700/j.0379-1726.1996.02.003

Yang, S. F., Chen, H. L., Ji, D. W., Li, Z. L., Dong, C. W., Jia, C. Z., et al. (2005). Geological process of early to middle Permian Magmatism in Tarim Basin and its geodynamic significance. *Geol. J. China Univ.* 11 (4), 504–511. (in Chinese with English abstract).

Yang, S. F., Chen, H. L., Li, Z. L., Li, Y. Q., Yu, X., Li, D. X., et al. (2013). Early permian Tarim large igneous province in northwest China. *Sci. China Earth Sci.* 56, 2015–2026. doi:10.1007/s11430-013-4653-y

Yao, Y. T., Zeng, L. B., Mao, Z., Han, J., Cao, D. S., and Lin, B. (2023). Differential deformation of a strike-slip fault in the Paleozoic carbonate reservoirs of the Tarim Basin, China. *J. Struc Geo* 173, 104908. doi:10.1016/j.jsg.2023.104908

Yi, S. W., Li, M. P., Guo, X. J., Fan, T. Z., Yang, F., Fang, H., et al. (2020). Control of the nanhua paleo-rift on cambrian sedimentation and its exploration significance in Tarim Basin. *Acta Pet. Sin.* 41 (11), 1293–1308. (in Chinese with English abstract). doi:10.7623/syxb202011001

Zhang, Z. S., Li, M. J., and Liu, S. P. (2002). Generation and evolution of Tazhong low uplift. *Pet. Explor. Dev.* 29 (1), 28–31. (in Chinese with English abstract). doi:10.3321/j.issn:1000-0747.2002.01.007

Zhu, G. Y., Chen, F. R., Li, Z. Y., Zhang, Y., Xing, X., Tao, X. W., et al. (2016). Discovery and basic characteristics of the high-quality source rocks of the cambrian Yuertusi Formation in Tarim Basin. *Nat. Gas. Geosci.* 27 (01), 8–21. (in Chinese with English abstract). doi:10.11764/j.issn.1672-1926.2016.01.0008

Zhu, G. Y., Hu, J. F., Chen, Y. Q., Xue, N., Zhao, K., Zhang, Z. Y., et al. (2022). Geochemical characteristics and formation environment of source rock of the Lower Cambrian Yuertusi Formation in well Luntan 1 in Tarim basin. *Acta Geol. Sin.* 96 (06), 2116–2130. (in Chinese with English abstract). doi:10.3969/j.issn.0001-5717.2022.06.014

Zhu, G. Y., Ren, R., Chen, F. R., Li, T. T., and Chen, Y. Q. (2017). Neoproterozoic Rift basins and their control on the development of hydrocarbon source rocks in the Tarim Basin, NW China. *J. Asian Earth Sci.* 150, 63–72. doi:10.1016/j.jseaes.2017.09.018